Monthly Notices
of the
ROYAL ASTRONOMICAL SOCIETY

MNRAS **478,** 758–783 (2018) doi:10.1093/mnras/sty1220

Photometric variability of TW Hya from seconds to years as seen from space and the ground during 2013–2017

Michal Siwak,[1]★ Waldemar Ogloza,[1] Anthony F. J. Moffat,[2] Jaymie M. Matthews,[3] Slavek M. Rucinski,[4] Thomas Kallinger,[5] Rainer Kuschnig,[5] Chris Cameron,[6,7] Werner W. Weiss,[5] Jason F. Rowe,[2] David B. Guenther[8] and Dimitar Sasselov[9]

[1]*Mount Suhora Astronomical Observatory, Cracow Pedagogical University, ul. Podchorazych 2, 30084 Krakow, Poland*
[2]*Département de Physique, Université de Montréal, C.P. 6128, Succursale: Centre-Ville, Montréal, QC, H3C 3J7, Canada*
[3]*Department of Physics & Astronomy, University of British Columbia, 6224 Agricultural Road, Vancouver, BC, V6T 1Z1, Canada*
[4]*Department of Astronomy and Astrophysics, University of Toronto, 50 St George St., Toronto, ON, M5S 3H4, Canada*
[5]*Universität Wien, Institut für Astrophysik, Türkenschanzstrasse 17, A-1180 Wien, Austria*
[6]*Department of Mathematics, Physics & Geology, Cape Breton University, 1250 Grand Lake Road, Sydney, NS, B1P 6L2, Canada*
[7]*Canadian Coast Guard College, Department of Arts, Sciences, and Languages, Sydney, NS, B1R 2J6, Canada*
[8]*Institute for Computational Astrophysics, Department of Astronomy and Physics, Saint Mary's University, Halifax, NS, B3H 3C3, Canada*
[9]*Harvard-Smithsonian Center for Astrophysics, 60 Garden Street, Cambridge, MA 02138, USA*

Accepted 2018 May 5. Received 2018 May 5; in original form 2018 February 28

ABSTRACT

This is the final photometric study of TW Hya based on new *MOST* satellite observations. During 2014 and 2017, the light curves showed stable 3.75- and 3.69-d quasi-periodic oscillations, respectively. Both values appear to be closely related to the stellar rotation period, as they might be created by changing visibility of a hotspot formed near the magnetic pole directed towards the observer. These major light variations were superimposed on a chaotic, flaring-type activity caused by hotspots resulting from unstable accretion – a situation reminiscent of that in 2011, when TW Hya showed signs of a moderately stable accretion state. In 2015, only drifting quasi-periods were observed, similar to those present in 2008–2009 data and typical for magnetized stars accreting in a strongly unstable regime. A rich set of multicolour data was obtained during 2013–2017 with the primary aim of characterizing the basic spectral properties of the mysterious occultations in TW Hya. Although several possible occultation-like events were identified, they are not as well defined as in the 2011 *MOST* data. The new ground-based and *MOST* data show a dozen previously unnoticed flares, as well as small-amplitude 11 min–3 h brightness variations, associated with 'accretion bursts'. We cannot exclude the possibility that the shortest 11–15 min variations could also be caused by thermal instability oscillations in an accretion shock.

Key words: stars: individual: TW Hya – stars: variables: T Tauri, Herbig Ae/Be.

1 INTRODUCTION

TW Hya was shown to be a genuine classical T Tauri type star (CTTS: Rucinski & Krautter 1983) in a young (about 7–10 Myr) association called TWA (Kastner et al. 1997; Barrado y Navascues 2006). It is one of the last two stars in the association that still show vigorous accretion (see the results of Tofflemire et al. 2017 for the young binary TWA 3A) and also the closest (59.5 pc, Gaia collaboration et al. 2016) T Tauri type star to us. The pole-on geometry of its transitional protoplanetary disc visibility (an inclination of 5–15° between the stellar rotational axis and the observer was derived for the star – see Rucinski et al. 2008 for a review and also Donati et al. 2011) favours TW Hya for detailed studies with modern imaging instrumentation: in addition to the previously known disc gap at 80 au found in *Hubble Space Telescope* (*HST*) images (Debes et al. 2013), Akiyama et al. (2015) found a gap localized in the disc at a Uranus distance of 20 au using the *Subaru* High-Contrast Coronographic Imager for Adaptive Optics (*Subaru*–HiCIAO). A most detailed image of TW Hya provided by the Atacama Large Millimeter/submillimeter Array (ALMA: Andrews et al. 2016) revealed numerous rings – the closest, localized at 1 au from the star, has popularly been interpreted as caused by an Earth-like planet sweeping disc matter in its orbit. Sophisticated, deep spectral differential imaging in the Paβ line looking for accretion signatures of possible planets was sensitive to 1.45–2.3 Jupiter-mass planets but did not reveal significant signals (Uyama et al. 2017). Similar

★ E-mail: siwak@oa.uj.edu.pl

upper limits at 1–2.3 Jupiter masses for planets expected to form in the four well-known gaps in the disc were placed from long-exposure L'-band coronographic imaging observations by Ruane et al. (2017). In addition to the above, Debes et al. (2017) analysed *HST* Space Telescope Imaging Spectrograph (STIS) images obtained over 18 years. These images reveal that the inner disc is likely inclined and precessing, blocking central starlight and casting a shadow on the more external disc parts. The shadow is moving coherently with a period of 15.9 yr.

In spite of superior modern instrumentation, investigation of the innermost disc dynamics is still possible only through photometry and spectroscopy. For instance, these old but well-established techniques enable insight into the properties of hotspots, which are the disc–plasma fingerprints on a star produced during magnetospheric accretion (Königl 1991). Photometric observations of TW Hya were started almost four decades ago and were primarily aimed at determining the rotational period of the star – the basic clock in the star–disc system. The first photometric results of Rucinski & Krautter (1983) and Rucinski (1988) were inconclusive: these authors were unable to find any stable periodicity. Although Mekkaden (1998) found a periodic value at 2.196 d, Herbst & Koret (1988) found two totally different but significant peaks at 1.28 and 4.5 d. Alencar & Batalha (2002) analysed the power spectrum of the veiling variations and obtained three major periodicities at 1.4 ± 0.1, 2.85 ± 0.25 and 3.75 ± 0.45 d. A similar study by Batalha et al. (2002) pointed to 4.4 ± 0.4 d as the stellar rotation period. The period of 2.80 d found by Lawson & Crause (2005) confirmed that no single value, coherent over many years, can be established from ground-based observations of this active star.

Explanation of this ambiguity was possible after the launch of *Microvariability & Oscillations of STars* (*MOST*) – the first space telescope dedicated to long-term, high-precision photometry of ∼0–12 mag stars (Walker et al. 2003; Matthews et al. 2004). Rucinski et al. (2008) observed TW Hya continuously for 11.4 and 46.7 d in 2007 and 2008, respectively. During the longer run, the star showed irregular 'shot-noise' or flaring-type activity, with typical amplitudes of about 0.5 mag, typical for Type II, irregular and accretion-burst classes, as defined by Herbst et al. (1994), Alencar et al. (2010), Cody et al. (2014) and Stauffer et al. (2014), respectively. Rucinski et al. (2008) found this flicker-noise character of the Fourier spectrum without any dominant periodicity – only during the 2007 observations did the star show a possibly stable 3.7-d quasi-period, but the run was too short to confirm this conclusion for definite. In the longer 2008 light curve analysed with the wavelet technique, the authors discovered a few quasi-periodic oscillations (QPOs) showing period shortening over the run. These findings were interpreted as possibly caused by condensed hot plasma clumps localized within range 15–2 $R_\odot$ in the disc, gradually moving on spiral orbits towards the star. Similar quasi-periodic oscillatory variations, which appeared in the accessible range of about 10–1.3 d and typically shortened their periods by a factor of two within a few weeks, were confirmed during the third, 40.3-dlong run by Siwak et al. (2011).

The results of the fourth set of 2011 *MOST* observations were exceptional when compared with those from the previous seasons (Siwak et al. 2014): while the overall light variations retained the general characteristics of flicker noise, the 2011 season variations did not show any obvious period shortening of oscillation features. This time, the Fourier and wavelet spectra were dominated by a single, almost stable oscillation with a period of 4.18 ± 0.25 d. We interpreted these findings within the framework proposed by Romanova et al. (2004), Romanova, Kulkarni & Lovelace (2008) and Romanova & Kulkarni (2009), in which the regime of accretion is responsible for a variety of light variations observed in magnetized stars, including CTTSs. According to these authors, the accretion regime can be stable, moderately stable or unstable at any particular time. Moreover, it can also alternate between different states, depending primarily on the temporary mass-transfer rate. The resulting light curves of a CTTS may change from (more or less) regular to (very) irregular, which also affects the Fourier spectra. The Fourier spectrum will be dominated by a single or two well-defined stable peak(s) if the accretion regime is stable. In this state, two antipodal high-latitude hotspots are produced by accretion funnels arising at the disc corotation radius and the peaks are expected to reveal the rotational period of the star. Once the mass accretion rate increases, instabilities start to appear at the *inner disc–magnetosphere* interface: the accretion regime becomes moderately stable and the Fourier spectrum shows additional frequencies arising from hotspots created by stochastic equatorial tongues of accreting plasma. The spectra will eventually become very noisy, without any dominant peaks during an unstable state of accretion. In this state, several QPOs may be produced simultaneously by hotspots revolving on a star with Keplerian frequencies of an inner disc. Their periods, being a fraction of a true rotational period of the star, may show considerable variations if the mass transfer rate inside the particular narrow tongue changes during its short lifetime (Kulkarni & Romanova 2009).

According to the above scheme, due to the absence of any stable periodicity in the 2008 and 2009 *MOST* light curves, we inferred that a strongly unstable regime of accretion, solely through fast-moving equatorial tongues, operated in TW Hya at the time. For the same reason, we proposed that the dominant oscillation in 2011 was caused by rotational modulation produced by a single, large hotspot formed by a stable accretion funnel and the fairly stable 4.18-d signal could represent the true rotational period of the star. However, it was not clear how the 4.18-d periodicity relates to the previously observed 3.57-d period in spectroscopic data by Donati et al. (2011). Inspired by this result, we continued monitoring of TW Hya with *MOST* during the 2014, 2015 and 2017 seasons.

Except for the fairly regular light variations, the 2011 *MOST* light curve showed a previously unnoticed feature: a series of semi-periodic, short (10–20 min) and shallow (2–3 per cent) well-defined dips, initially interpreted as caused by occultations of hotspots by hypothetical 'dusty clumps'. As the dips were observed during one season only and through the *MOST* filter that integrates almost the entire visual spectrum, we decided to characterize their spectral properties using Johnson and Sloan filters. We describe multicolour observations obtained during 2013–2017 at the South African Astronomical Observatory (SAAO) and Cerro Tololo Inter-American Observatory (CTIO) in Section 2. In the same section we describe observations of two new instances of the moderately stable accretion state in TW Hya, which apparently took place in 2014 and 2017 and were observed by *MOST* during the fifth and seventh series of observations. The sixth 2015 run revealed only drifting QPOs, typical for an unstable accretion state. We analyse these new data and immediately discuss the results obtained in Section 3. A summary of the major results is given in Section 4.

2 OBSERVATIONS AND DATA REDUCTION

2.1 *MOST* observations

The optical system of the *MOST* satellite consists of a Rumak–Maksutov *f*/6, 15 cm reflecting telescope. The custom broad-band 'white' filter covers the spectral range 370–750 nm with effective

wavelength located close to the Johnson *V* band. The pre-launch characteristics of the mission are described by Walker et al. (2003) and the initial post-launch performance by Matthews et al. (2004).

The three new runs of nearly contiguous TW Hya observations, utilizing the *direct-imaging* data-acquisition mode, took place over the following periods:

(i) 41.52 d between 2014February 25 and April 7, during 514 satellite orbits,
(ii) 21.88 d between 2015 March 25 and April 15, during 299 satellite orbits, and
(iii) 28.18 d between 2017 March 3 and 28, during 295 satellite orbits.

Because the star is not in the Continuous Visibility Zone of the satellite and some short time-critical observations of other targets were performed in parallel, the effective total time coverage was 8.59, 7.59 and 5.87 d, i.e. 20.7, 34.7 and 20.8 per cent of each run's total length, respectively.

The individual exposures were 60 s long during the first 5.51 d of the 2014 run and 120 s for the rest, including the 2015 and 2017 runs. Aperture photometry of the stars was obtained using RAW images by means of the DAOPHOT II package (Stetson 1987). As in our previous investigations, a weak correlation between the stellar flux and the sky background level within each *MOST* orbit was noted and removed; this was most probably caused by a small photometric non-linearity in the electronic system. Due to the lack of availability of *flat-field* and *dark* calibration images, we also removed the small correlation between the star brightness and its point-spread function centroid position in the subrasters.

We obtained three well-defined light curves for almost the whole duration of the observations (Fig. 1). The typical error of a single data point is about 0.011 mag. The median value of the scatter (σ) of 514 averaged 2014 data points (formed for each satellite orbit of 101 min) is 0.0082, with the full range between 0.0002and 0.0329 in units of the mean normalized flux for the star. The median value of the scatter of the 2015, 299 averaged data points was 0.0087, with a full range of 0.0031–0.0503, while in the case of the 2017, 295 averaged data points the respective values are equal to 0.0064 and 0.0021–0.0335 in units of the mean normalized flux for the star – the values of scatter include the variability intrinsic to the accretion, occurring on time-scales shorter than the length of a single *MOST* orbit.

Unfortunately, the 2014 data were interrupted five times to conduct observations of other time-critical targets. In addition, the effective coverage time within single orbits became significantly lower after heliocentric Julian date HJD $\approx$ 245 6731. The 2015 data were interrupted only once, while three major interruptions affected the 2017 data to a certain extent, especially the longest one at HJD $\approx$ 245 7837. These facts have a negative influence on the investigation of the shortest periods using the wavelet technique. We also note that the long on-board stacking intervals of 120 s used for the majority of the new *MOST* data seriously limited new searches for short-lasting 'occultations'.

2.2 Multicolour observations

2.2.1 SAAO *2013 I: the Sloan* g′r′i′*-filter data from the 0.75-m telescope*

We started ground-based monitoring of TW Hya at the South African Astronomical Observatory (SAAO). The first data were obtained on 2013 April 11/12 and the last on 2013 May 7/8. The total run length was 26.17 d. Observations were gathered during 22 nights of different length and photometric quality. The observing log is provided in Table 1.

We used the 0.75-m telescopeequipped with TRIPOL, which is the visitor instrument of Nagoya University donated to the SAAO. With the 11.75-m telescopefocal length, the field of view is 3 × 3 arcmin^2. The light is split by two dichroics, then directed to three SBIG (Santa Barbara Instruments Group) *ST-9XEI* CCD cameras through the Sloan $g'r'i'$ filters, resulting in three simultaneous images for each exposure. The cadence of our observations was very high and ranged between 8 and 23 s (including 3 s readout time), depending on the actual seeing. All frames were *dark* and *flat-field* calibrated in a standard way using our scripts written in the MIDAS package (Warmels 1991). For photometric reduction we used the C-MUNIPACK software (Motl 2011), which utilizes the DAOPHOT II package.

In Fig. 2(a) we present g'- and r'-filter light curves obtained relative to the 'mean comparison star' formed from the fourth and fifth stars listed in Table 2. We do not show the i'-filter data, which are affected by incomprehensible instrumental trends occurring each night. We stress that the only two available comparison stars are significantly fainter than TW Hya, which strongly affects the quality of the final light curves. Therefore, for studies of subtle light changes in TW Hya we used just the pure photometric measurements of the star, obtained during 13 fully or partly photometric nights. These data were corrected for nightly trends using mean extinction coefficients for the corresponding filters determined for SAAO, as described in Appendix A. We show the 2013 data obtained during photometric nights in detail in Appendix B (Fig. B1).

2.2.2 SAAO *2013 II: the Johnson* BV*-filter observations from the 0.5-m telescope*

We also observed TW Hya from 2013 December 4–2014 January 14, using the single-channel *Modular* photometer on the 0.5-m *Boller & Chivens* telescope. The run was shared with multicolour observations of FU Ori, which were performed simultaneously with *MOST* during the first halves of the nights, until TW Hya rose high enough above the horizon for accurate measurements. However, during most nights we struggled significantly with bursts of high humidity, eventually leading to the formation of ridge clouds over the observatory just after midnight. We were able to observe TW Hya in *BV* filters continuously for a few hours only during a few nights. We do not present these light curves, as the way they were collected (without frequent sky-level and comparison-star measurements) was focused on the detection of short-duration 10–20 min occultations. Unfortunately, the results were negative.

2.2.3 CTIO *2014 and 2015: the Sloan* u′g′z′*-filter data from the 0.9-m* SMARTS *telescope*

In 2014 we joined the Small & Moderate Aperture Research Telescope System (SMARTS) and observed TW Hya on two occasions: for the first time during 15 nights from 2014 March 6–20 and for the second time during 14 nights from 2015 March 4–17 – this run was coordinated with the SAAO run on the 1-m telescope (see below in Section 2.2.4). The 2014 run was performed simultaneously with the *MOST* observations. The total run durations were 14.35 and 13.38 d, respectively.

We used the 0.9-m telescope, which is equipped with a Tek2K 2048 × 2046 pixel CCD camera and a set of Sloan $u'g'r'i'z'$

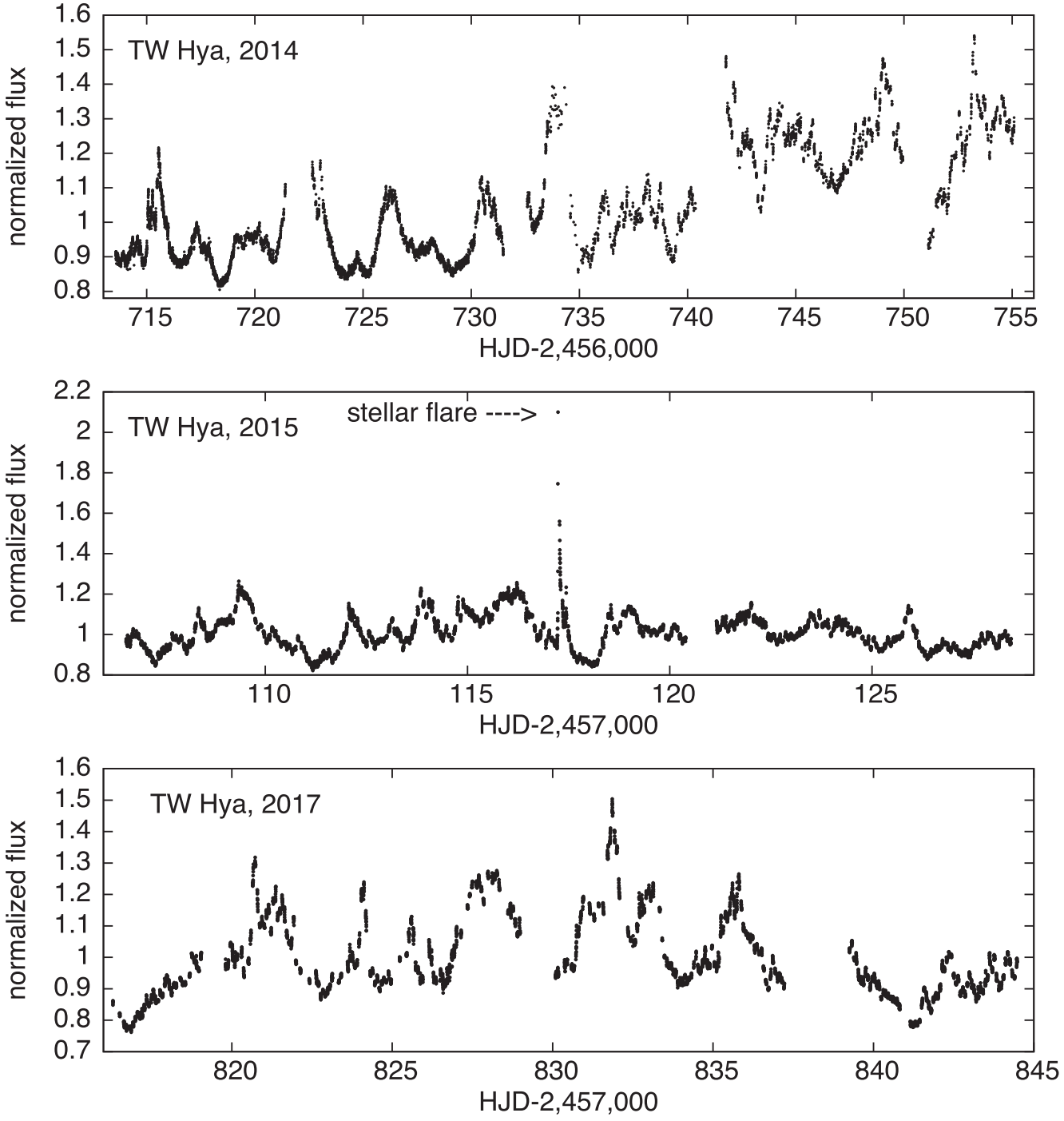

Figure 1. The 2014, 2015 and 2017 *MOST* light curves of TW Hya in flux units, scaled to unity at the mean brightness level, which was different for each year.

filters. With the scale of 0.401 arcsec pixel^{-1}, the field of view is 13.6 × 13.6 arcmin^2. To decrease the readout time, we have reduced the field of view to 6.8 × 6.8 arcmin^2 and used two amplifiers. As the camera is cooled down to −120 °C with liquid nitrogen, *dark* frames were not necessary. All further calibrations of *bias* and *flat-field* were made in the same way as for the *SAAO* data.

A 'mean comparison star', calculated from two very stable (to 0.01 mag in all filters over all five years) stars in the field (the first and third stars listed in Table 2), was used for differential photometry. The light curves constructed from all-night observations are shown in Figs 2(b) and (d).

In 2014 the $u'g'z'$ filters were used. The observations in the z' filter were obtained with the hope of detection of cold-spot-induced modulations in the light curve, but the result was negative – accretion effects, which dominate in the $u'g'$ filter data, are still pronounced near 9000 Å, though with amplitudes considerably scaled down. Therefore, after the first three nights in 2014 we limited observations in this band considerably to increase the sampling rate in the most

Table 1. The extended log of *MOST,* SAAO and CTIO observations. Special features noticed during particular nights, i.e. flares (and their major parameters with errors in brackets) and possible occultations are listed.

Date	Filters	Flare HJD_{max}; $T_{0.5}$ [min]; U_{max} [norm flux]	'Occultation'
2013-04-11	$g'r'i'$	–	–
2013-04-12	$g'r'i'$	–	possibly
2013-04-13	$g'r'i'$	–	–
2013-04-14	$g'r'i'$	–	possibly
2013-04-15	$g'r'i'$	–	–
2013-04-18	$g'r'i'$	–	
2013-04-19	$g'r'i'$	–	–
2013-04-20	$g'r'i'$	–	–
2013-04-21	$g'r'i'$	–	–
2013-04-22	$g'r'i'$	–	–
2013-04-23	$g'r'i'$	–	–
2013-04-24	$g'r'i'$	–	–
2013-04-25	$g'r'i'$	–	–
2013-04-26	$g'r'i'$	–	–
2013-04-27	$g'r'i'$	–	–
2013-04-28	$g'r'i'$	–	–
2013-04-29	$g'r'i'$	–	–
2013-04-30	$g'r'i'$	–	possibly
2013-05-01	$g'r'i'$	–	–
2013-05-02	$g'r'i'$	–	–
2013-05-04	$g'r'i'$	–	–
2013-05-05	$g'r'i'$	–	–
2013-05-06	$g'r'i'$	–	–
2013-05-07	$g'r'i'$	–	–
2014-02-24 : 04-11	'white'	–	–
2014-03-06	$u'g'z'$	–	–
2014-03-07	$u'g'z'$	–	–
2014-03-08	$u'g'z'$	–	–
2014-03-09	$u'g'z'$	flare or an accretion burst at 245 6726.8340	–
2014-03-10	$u'g'z'$	–	possibly
2014-03-11	$u'g'z'$	245 6728.8864(3); 10.7(2.5); 1.17(3)	–
2014-03-12	$u'g'z'$	–	possibly
2014-03-13	$u'g'z'$	–	–
2014-03-14	$u'g'z'$	–	–
2014-03-15	$u'g'z'$	–	–
2014-03-16	$u'g'z'$	flare or an accretion burst at 245 6733.7075	–
2014-03-17	$u'g'z'$	–	–
2014-03-18	$u'g'z'$	–	–
2014-03-19	$u'g'z'$	–	–
2014-03-20	$u'g'z'$	–	possibly
2015-03-04	$UBVu'g'$	flare or an accretion burst at 245 7086.8121	–
2015-03-05	$UBVu'g'$	flare or an accretion burst at 245 7087.6698	–
2015-03-06	$UBVu'g'$	–	–
2015-03-07	$UBVu'g'$	–	–
2015-03-08	$UBVu'g'$	no.1: 245 7090.5959(3); 2.5(1.5); 0.66(1) no.2: flare or an accretion burst at 245 7090.6696	–
2015-03-09	$UBVu'g'$	245 7091.5754(2); 1.5(1.5); 0.15(1)	–
2015-03-10	$UBVu'g'$	–	–
2015-03-11	$UBVu'g'$	245 7093.5483(3); 2.9(1.5); 0.06(1)	possibly
2015-03-12	$UBVu'g'$	flare or an accretion burst at 245 7094.8085	–
2015-03-13	$UBVu'g'$	–	–
2015-03-14	$UBVu'g'$	–	–
2015-03-15	$UBVu'g'$	–	–
2015-03-16	$UBVu'g'$	–	–
2015-03-17	$UBVu'g'$	245 7099.7902(2); 7.2(1.5); 0.065(5)	–
2015-03-25 : 04-15	'white'	no.1: 245 7117.245(2); 50(10) ; >1.24 no.2: 245 7117.4384(3); 4.0(5); 0.12(1)	–
2016-02-23	UBV	–	–
2016-02-24	UBV	–	–
2016-02-25	UBV	–	–

Table 1 – *continued*

Date	Filters	Flare HJD_{max}; $T_{0.5}$ [min]; U_{max} [norm flux]	'Occultation'
2016-02-26	*B*	–	–
2016-02-27	*UBV*	–	–
2016-02-28	*UBV*	two flares or accretion bursts at 245 7447.555	–
2016-02-29	*UBV*	–	–
2016-03-01	*UBV*	–	–
2016-03-02	*UBV*	–	–
2016-03-03	*UBV*	no.1: 245 7451.5333(5); 5.2(1.5); 0.13(1) no.2: 245 7451.5822(5); 3.3(1.5); 0.13(1)	–
2016-03-04	*UBV*	–	–
2016-03-06	*UBV*	–	–
2016-03-07	*UBV*	–	–
2016-03-08	*UBV*	–	–
2016-03-09	*UBV*	–	–
2016-03-10	*UBV*	–	–
2016-03-12	*UBV*	–	possibly
2016-03-13	*UBV*	245 7461.3981(7); 7.5(1.5); 0.29(1)	–
2016-03-14	*UBV*	–	–
2016-03-15	*UBV*	–	–
2017-03-03:28	'white'	–	–
2017-03-08	$u'g'r'$		–
2017-03-09	$u'g'r'$	–	–
2017-03-10	$u'g'r'$	–	–
2017-03-11	$u'g'r'$	–	–
2017-03-12	$u'g'r'$	–	–
2017-03-13	$u'g'r'$	–	–
2017-03-14	$u'g'r'$	–	–
2017-03-15	$u'g'r'$	–	–
2017-03-16	$u'g'r'$	–	–
2017-03-17	$u'g'r'$	245 7830.361(1); 3.5(1.5); 0.42(3)	–
2017-03-18	$u'g'r'$	–	–
2017-03-19	$u'g'r'$	–	–
2017-03-20	$u'g'r'$	–	–
2017-03-21	$u'g'r'$	–	–

detail-rich $u'g'$ filters. We skipped the z' filter totally during the 2015 run.

We show the 2014 and 2015 observations in detail in Appendix B (Figs B2 and B3). The data shown in these figures were left uncorrected for atmospheric extinction. This is due to the fact that proper treatment of the dominant colour extinction term requires actual values of the $u' - g'$ colour index, whilst during a few nights the u' filter was skipped for several hours during poor seeing conditions and/or passing clouds. No transformation to the standard system was made and the data were left in the instrumental system.

2.2.4 *The 2015 and 2016* UBV *and the 2017* u′g′r′ SAAO *light curves from the 1-m telescope*

Encouraged by the 2014 CTIO results, in 2015 we decided to increase the effective coverage using the SAAO 1-m *Elizabeth* telescope. This telescope is equipped with a STE4 1024 × 1024 pixel CCD camera and a set of Johnson–Bessel *UBVRI* filters. *UBV* filters have been used to cover a spectral range similar to that covered by the Sloan $u'g'$ filters at CTIO. The 2015 SAAO run was strictly coordinated with the CTIO observations, which allowed us to reduce daily breaks to 10–11 h.

To reduce the read-out time to 17 s per frame, we binned the chip to 512 × 512 pixels; at the same time, the stellar point-spread function was still well sampled with 0.31 arcsec pixel^{-1} resolution. All reduction steps were made in the same way as for the previous CCD observations. The first and second comparison stars were used for differential photometry in 2015 (see Table 2). The data were left in the instrumental system, but were later corrected to colour extinction terms (see in Appendix A) to prepare colour–magnitude diagrams. The *UBV* light curves constructed from all-night observations are shown in Fig. 2(c). The data obtained during all photometric nights are shown in Appendix B (Fig. B4).

The major limitation of the combined run was the use of two different photometric systems. However, we decided to keep the use of the Sloan filters at CTIO, which has the huge advantage of higher and nearly flat peak transmission curves with better defined profiles, making each band practically independent from the other – this advantage was very important to characterize the short-term occultations. The only simple combination of light curves obtained from both sites was possible for the u' and U filters, as their transmission functions are very similar. We found that variability amplitudes in the two data sets overlapping for 1–3 h are almost identical (to 0.005 mag) and the combined light curves can be treated as an (almost) homogeneous set of data. The combined u-band 2015 light curve (corrected for colour extinction effects) is shown in Fig. 2(e).

The second run on the 1-m *Elizabeth* telescope utilizing Johnson filters was performed during 22 nights from 2016 February 23–March 15; the results are shown in Fig. 2(f) and in Appendix B

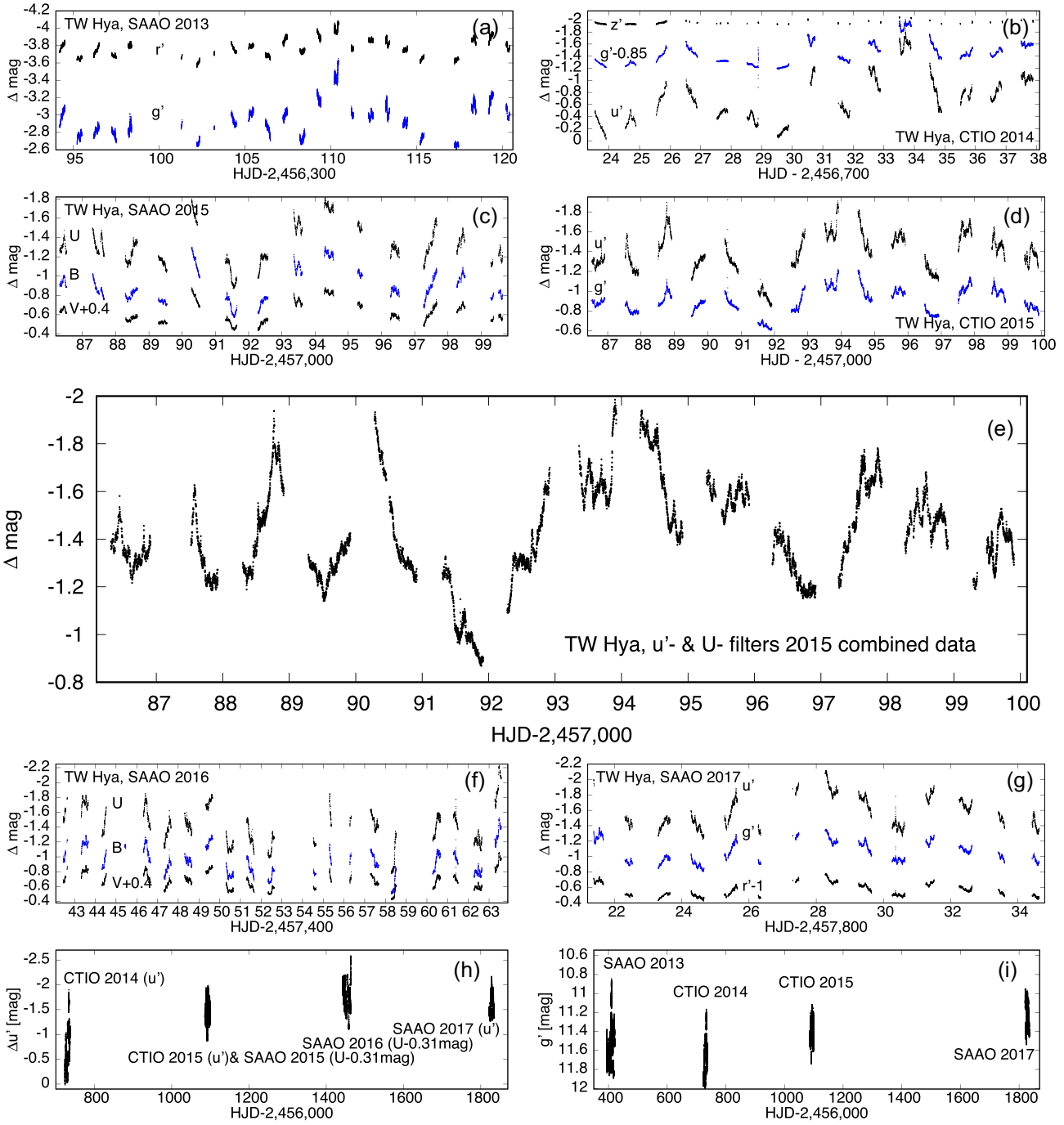

Figure 2. The ground-based light curves of TW Hya obtained during 2013–2017. The years, sites and filters are labelled in consecutive panels. The large middle panel shows the 2015*u*-band light curve, composed of the *CTIO* u'-filter and the *SAAO* *U*-filter data. The two bottom panels show the long-term brightness evolution in the u' and g' filters – the last light curve was roughly calibrated to the standard Sloan system.

(Fig. B5). The total run duration was 21.13 d. During this run, we included in the field of view the most stable comparison star, listed as the third one in Table 2. This enabled us to align the 2015 and 2016 SAAO light curves for display purposes and presentation of uniform colour–magnitude diagrams (Section 3.6). Unfortunately a simultaneous run at CTIO was impossible at that time.

The third and last run on the *Elisabeth* telescope took place from 2017 March 8–21. It was 13.25 d long and was performed simultaneously with the third *MOST* satellite run and with high-cadence low-resolution spectroscopic monitoring of TW Hya by means of the 1.9-m SAAO telescope. The combined spectroscopic and photometric results will be the subject of a separate publication. In 2017, we used the first opportunity to observe the star in $u'g'r'$ Sloan filters. The same detector, binning and reduction processes were used: the final light curve is shown in Fig. 2(g), while data obtained during nights with stable weather conditions are shown in

Table 2. The comparison (cmp) and the control (chck) stars used for differential photometry of TW Hya over 2013–2017. The magnitudes of the first star are from the RAdial Velocity Experiment (RAVE) project (Munari et al. 2014). TYC 7208-1422-1 and USNO-A2 0525-13705888 were usually used to compute a 'mean comparison star'. RAVE J110143.8-343930 played the role of the comparison star only during the 2015 SAAO run.

star	B	V	g'	r'	i'	2013	2014	2015	2016	2017
TYC 7208-1422-1	12.781(16)	11.964(16)	12.333(8)	11.720(14)	11.461(23)	–	cmp	cmp	cmp	cmp
RAVE J110143.8-343930	–	–	–	–	–	–	chck	chck,cmp	chck	chck
USNO-A2 0525-13705888	–	–	–	–	–	–	cmp	cmp	cmp	cmp
USNO-A2 0525-13705192	–	–	–	–	–	cmp	–	–	–	–
USNO-A2 0525-13705637	–	–	–	–	–	cmp	–	–	–	–

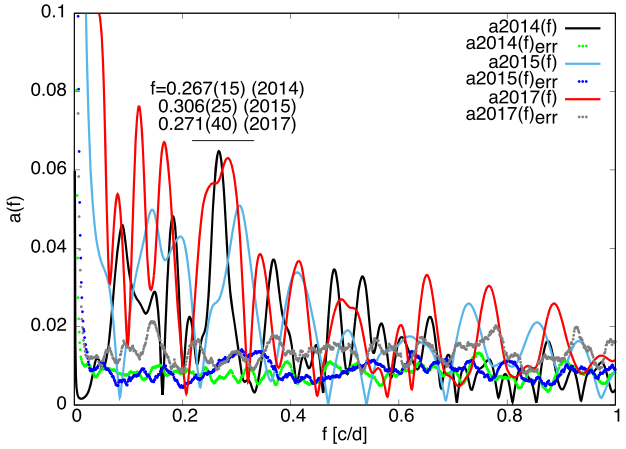

Figure 3. The Fourier spectra of three *MOST* light curves. The peaks indicating the approximate value of the stellar rotational period are underlined and their respective central frequencies are shown.

Appendix B (Fig. B6). The most reliable first and third comparison stars (Table 2) formed the 'mean comparison star'.

3 ANALYSIS OF ALL DATA AND DISCUSSION OF THE RESULTS

3.1 Fourier analysis of *MOST*, SAAO and CTIO light curves

We performed analysis of the new light curves in the same way as in Rucinski et al. (2008) and Siwak et al. (2011, 2014, 2016). The bootstrap sampling technique permitted evaluation of the mean standard errors of the amplitude $a(f)$, where f is the frequency. Due to the different sampling rates per orbit over the 2014 run, we used mean-orbital data points during the analysis. The 2015 and 2017 frequency power spectra were calculated in the same way for uniformity.

The 2014 Fourier spectrum (Fig. 3) shows one stable peak centred at 0.267 ± 0.015 cd^{-1} (3.75 d). A similar peak appears in the 2015 Fourier spectrum (0.306 ± 0.025 cd^{-1}, i.e. 3.27 d), but its stability will be questioned later on the basis of the wavelet-analysis result. The 2017 data show a stable peak at 0.271 ± 0.040 cd^{-1} (3.69 d). Note that the error in the frequency of the peak is large, as the peak likely consists of two close overlapping features. We also note that lower-frequency peaks, which indicate 5–10 d oscillations, are present in the Fourier spectra but they do not represent significant periodic variations based on the light curves themselves.

Taking into account our previous *MOST* achievements for TW Hya, attempts to search for periodic signals a few days long in light curves affected by daily breaks and non-uniform weather patterns may appear to be irrational. In spite of these concerns, we found some evidence of quasi-periodicities centred as follows:

(1) 3.15 d in the 4-week long 2013 SAAO $g'r'$ data set,
(2) 3.64 d in the 2-week long 2014 CTIO $u'g'z'$ data set,
(3) 4.44 d in the combined SAAO U- and CTIO u'-filter data sets,

although this value lies at the limit of what can be considered as a real quasi-periodic signal from the 13.588-d run,

(4) 3.45 d in the 3-week long 2016 SAAO UBV data set and
(5) 3.46 d in the 2-week long 2017 SAAO $u'g'r'$ data set.

The peaks in the frequency amplitude spectra obtained from ground-based data are usually wide and not symmetric. This can be caused by the period drift of the dominant QPO over a run, as clearly observed in many *MOST* runs (see below) and due mostly to limited temporal coverage. Although we show the results with precision to the second decimal place, the real uncertainties of these values are $\sim 0.2-0.3$ d. Nevertheless, they are in accordance with our previous and current *MOST* observations, which indicate firmly that the stellar rotational period must be close to the spectroscopic value 3.57 d of Donati et al. (2011).

3.2 Wavelet analysis of the *MOST* data

To obtain the uniform data sampling required for the wavelet analysis and to remove a few interruptions in the data acquisition (see Section 2), we interpolated with splines the 514 (2014), 299 (2015) and 295 (2017) mean satellite-orbit flux points into a grid of 589, 311 and 399 equally spaced points at 0.07046 d intervals, respectively. As a result, the gaps in the data acquisition were filled up with artificial points with uniform sampling like the rest of the data. As we found previously (Rucinski et al. 2008; Siwak et al. 2011, 2014, 2016), the Morlet-6 wavelet provided the best match between the time-integrated power spectrum and the original frequency spectrum of the star. The reliable two-dimensional oscillation wavelet spectrum (Fig. 4) is contained between the two white broken lines. Another limitation in our wavelet results is due to the four (2014), single (2015) and three (2017) interruptions in the data acquisition: the regions obviously affected by these breaks lie inside the small trapezium areas defined by white continuous lines. Unfortunately, the small trapezium areas may in fact propagate to longer periods and affect the wavelet spectra to an unknown degree. Therefore detailed visual inspection of the respective light curves is always necessary in order to verify whether a particular signal can be treated as real or not.

The new results comply with those obtained during the 2007, 2008, 2009 and 2011 *MOST* observations.

(i) The 2014 and 2017 data show stable signals at 3.75 and 3.69 d, in both the wavelet and the Fourier spectrum. This result is similar to that obtained recently from the 2011 data, where a stable 4.18-d

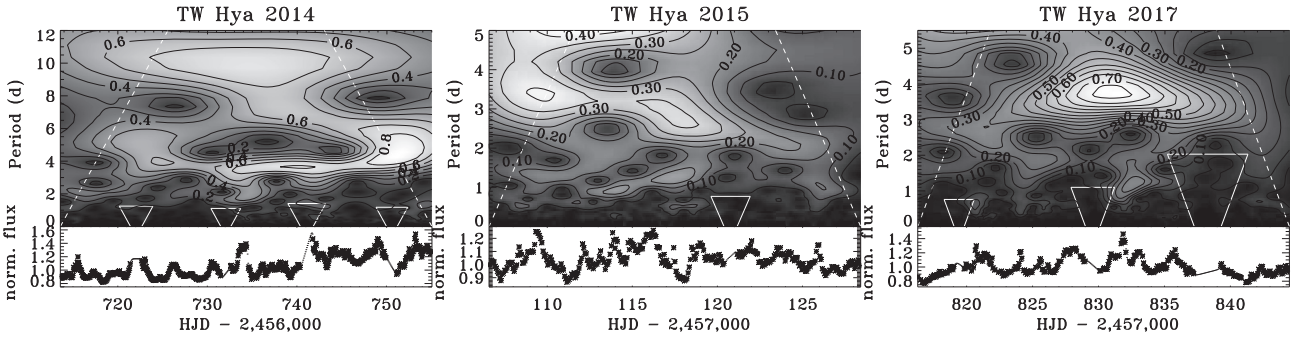

Figure 4. Wavelet spectra (upper panels) computed from a uniformly distributed time-grid with 0.07047 d spacing. The *MOST* data (in normalized flux units) are shown in the bottom panels as asterisks for quick cross-identification of the variability. The small dots indicate the interpolated gap-filling fragments of these light curves.

quasi-periodic modulation of large amplitude was observed for most of the run (Siwak et al. 2014).

(ii) In contrast to the previous results, the major peak at 0.306 cycle d^{-1} in the 2015 frequency spectrum does not appear as a stable feature in the wavelet spectrum – it shows period shortening between ∼3.4 and 2.2 d, similar to that observed in this star during the 2008 and 2009 *MOST* runs (Rucinski et al. 2008; Siwak et al. 2011).

We briefly conclude that the new results are in line with the picture outlined from our last *MOST* observations (Siwak et al. 2014) – the star apparently shows episodes of unstable (in 2015) and moderately stable accretion (in 2014, 2017), which determine the appearance of the light curves (Kurosawa & Romanova 2013). The period values observed this time (3.75 and 3.69 d) are closer to the spectroscopic value of the rotational period at 3.57 d by Donati et al. (2011). Thus, the periods observed by *MOST* do not appear to be 'false' periods caused by rotational modulation of hotspots created by an *ordered unstable regime*, discovered by Blinova, Romanova & Lovelace (2016). Instead, the almost-stable quasi-periodicities seen in 2014 and 2017 could be produced by rotational modulation in visibility of a large hotspot, created at the footprint of a steady accretion funnel striking the star close to its magnetic pole. The smaller peaks in the light curves could then be caused by hotspots formed at moderate stellar latitudes by equatorial tongues.

In addition to the above framework, the 'accretion burst' stochastic appearance and triangular shape of many peaks, already noticed in TW Hya by Rucinski et al. (2008), could also be the result of inhomogeneous accretion, characterized in detail by Gullbring et al. (1996). Some of the 'bursts' could also be explained by the development of shocks in the accretion columns due to smooth density variations in an inner disc (Robinson et al. 2017). The authors proposed that the shocks amplified in an accretion column can propagate along it and ultimately hit the star, leading to rapid, large-amplitude changes in the accretion rate. They obtained 'sawtooth' burst-profiles, with a rapid increase in brightness followed by a slower decline. Examination of the new *MOST* light curves reveals a few possible instances of such behaviour during 2015, although generally symmetrical 'triangular' profiles dominate in all *MOST* data.

3.3 Long-term evolution in ground-based data

To illustrate the long-term brightness evolution of TW Hya, we utilized the favoured g'- and u-band light curves (Fig. 2, bottom panels). For homogeneous calibration, all g'-filter data were recalculated with respect to the well-calibrated comparison star TYC 7208-1422-1 (Munari et al. 2014). The 2013 g'-filter light curve had to be aligned to those from 2014–2017 using shifts determined from the CTIO observations.

Long-term evolution in the u band can only be presented with respect to comparison stars. The two Johnson U light curves obtained at SAAO were shifted by 0.31 mag (as obtained from the 2015 data) to match the Sloan u' magnitude level, as indicated on the panel. No shift was applied to the 2017 SAAO u'-filter data. Corrections for colour extinction effects (see Appendix A) were applied to all these light curves. We stress that the data were obtained by means of three photometric systems, with unknown transformation equations to the standard system. We roughly estimated that this deficiency may lead up to 0.05 mag year-to-year deviations. This is fortunately a small effect, given the large amplitude of these long-term light changes – during four years, the average brightness level in the u band changed by about 1 mag and was followed by similar changes in the g' filter, but of smaller, 0.3 mag, amplitude. Similar changes were noted in the 2001–2008 All Sky Automated Survey (ASAS) V-filter data for TW Hya by Rucinski et al. (2008).

It is possible that the long-term changes could be related to the variation of the mean mass-accretion rate. When it increases, the inner disc becomes a source of many instabilities. According to Romanova et al. (2008), numerous unstable tongues of plasma are then formed, which eventually hit the star, leading to increased hotspot number along with associated veiling and mean-seasonal stellar brightness increases. Thus, just like the daily and weekly variations, the yearly variations also show the largest amplitudes in the u band. This view may be partially confirmed in the 2014 data, when the averaged brightness in the g' band was the lowest in 5 years and the *MOST* data analysed with the wavelet technique indicated a moderately stable regime. However, the same state was found in 2017 when unstable accretion operated in the star, while the average g'-band star brightness was even higher than during 2015. Longer continuous monitoring sessions, supported by independent mass accretion rate estimations, should be performed to examine the legitimacy of the aforementioned numerical scenario for explaining the long-term changes common for many actively accreting CTTSs. We note that other effects like variable circumstellar extinction may also come into play (Grankin et al. 2007). However, this last possibility seems to be unlikely for our target, as the dust extinction towards TW Hya has been estimated to be negligible by Herczeg et al. (2004).

3.4 Flares – the rate, amplitudes and durations

In contrast to our previous observations, the 2015 *MOST* and ground-based light curves revealed at least 12 flares of different

amplitudes and shape. In order to characterize their properties in a uniform way, we removed the underlying accretion-driven light variations using low-order polynomials. We then expressed intensities of the flares in flux units normalized to unity at the underlying continuum, as shown in Fig. 5. Based on the plots, we measured their major properties i.e. the start, maximum, end, half-duration ($T_{0.5}$) times and the *u*-band amplitudes $U_{\max}$ (if possible) – the most crucial parameters are shown in Table 1. Based on the parameters, one can divide observed flares of TW Hya into three (or possibly four) families.

(i) The first, single-member family consists of the 'super-flare' of 1 mag amplitude in the 'white' filter, lasting about 8 h and observed by *MOST* in 2015 (Fig. 5f). Unfortunately, we do not have *u*-band observations of the flare (where the amplitude could reach 5 mag). We note that TW Hya is not in the Continuous Viewing Zone of the satellite and the data acquisition must be interrupted for a dozen minutes during each satellite orbit. Therefore the peak of the flare was likely missed and the $T_{0.5}$ parameter is determined with low precision.

(ii) The second family consists of six flares with fast 1–2min rise times and purely exponential decays, as observed during 2014-03-11/12 (Fig. 5a), 2015-03-08/09 (Fig. 5b), 2015-03-17/18 (Fig. 5e), 2016-03-03/04 (Fig. 5g – the first event during the night), 2016-03-13/14 (Fig. 5h) and 2017-03-17/18 (Fig. 5i). Their *u*-band half-duration times are 2.5–10 min, with amplitudes of 0.065–1.17 in normalized flux units (0.07–0.85 mag). The second 2015 *MOST* flare likely also belongs to this family, due to its short half-duration time and low 0.12 (in normalized flux units) amplitude in the 'white' filter of the satellite.

(iii) The third family consists of very short flares called 'flashes', most pronounced in *U* and u' filters. They are barely distinguishable from the photon noise in the g' and *B* filters. The 'flashes' were observed on 2015-03-09/10 (Fig. 5c), 2015-03-11/12 (Fig. 5d) and 2016-03-03/04 (Fig. 5g – the second event during the night). One of them was observed simultaneously from two sites in 2015, which ruled out the originally considered 'cosmic ray' scenario. Their *u*-band amplitudes are 0.04–0.15 (in normalized flux units) and their half-duration times are 1.5–3.3 min. We stress that these estimates are uncertain due to the cadence of our observations being only twice as high as the lifetimes of the 'flashes'.

(iv) We also observed several events that cannot be classified as flares with any certainty. Although they seem to have similar amplitudes and duration times, as well as similar rise and decay times to flares assigned to the second family, they do show smaller differences between amplitudes seen in the $u'g'$ and *UBV* filters. In many respects they resemble 'accretion bursts', common for CTTSs (see below). We also indicate these phenomena in Table 1.

As far as we know, this is probably the first study of flares in TW Hya at visual wavelengths. Prior to the start of this investigation of their occurrence rate in 2007–2017, one must keep in mind that different photometric systems were used over these years. Additionally, the detection efficiency of flares by *MOST* (2007, 2008, 2009, 2011, 2014, 2015, 2017) was always reduced due to interruptions in the data acquisition during each orbit. Another limitation is imposed by the *MOST* filter, integrating almost whole visual light, which means that small-amplitude flares (maximum 10 per cent in the *u* band) could have been overlooked.

Because of the above, more general conclusions can be only drawn from analysis of ground-based data. We did not detect any flares or flashes during the 2013 observations. In 2014 we observed only a single flare during an effective monitoring time of 5.358 d, but in 2015 we recorded five flares at two observatories during 8.524 d – the two *MOST* flares were excluded from this statistic, as they were observed by an instrument of different sensitivity. Three flares were observed during the 2016 SAAO run, which effectively lasted for 5.308 d, while only one was observed in the 2017 run, which lasted for 4.026 d. When weighted by effective monitoring times, the occurrence rate during 2013, 2014, 2015, 2016 and 2017 was 0, 0.19, 0.59, 0.57 and 0.25 flare per day, respectively. If events marked in Table 1 as 'flares or accretion bursts' are included into this statistic, the respective rates are 0, 0.56, 0.94, 0.94 and 0.25 flare per day. Despite the flare activity perhaps being higher during the 2015 and 2016 runs, this result may be not significant, as the star was usually observed for a fraction of a month only. We conclude that further observations must be performed to be able to reach any viable conclusion about the flaring rate in TW Hya.

3.5 Analysis of multicolour 'accretion burst' dominated light curves

3.5.1 General description of the variability

In Appendix B, we present observations gathered at SAAO and CTIO during photometric or partly cloudy nights (which turned out to provide good-quality photometry anyway after careful reduction). Except for stellar flares, which can be distinguished well due to their characteristic fast rise time and slow exponential decay (Section3.4), these data show a variety of light changes at almost all times. They appear to be irregular, but exceptions from this general rule are indicated on some nights. The highest amplitudes are observed in the *u* band and they decrease with increasing effective wavelength of consecutive bands – e.g. the r'- and z'-filter light curves show considerably less variation and lower amplitudes than the accompanying $u'g'$-filter light curves.

The most pronounced variations, namely 'accretion bursts' as specified by Gullbring et al. (1996), are of 'triangular' shape. Their rise and decay branches last for similar times and they are well isolated from underlying smooth light variations occurring on longer time-scales (e.g. on 2013 April 13). 'Accretion bursts' may appear once, several times, or not at all during a night. They clearly avoid low brightness states, when accretion activity is significantly reduced (e.g. on 2013 April 25). Sometimes they are observed in close pairs (e.g. on 2013 April 13 and 14) and appear to be double-peaked, with a separation between consecutive maxima of a dozen minutes. Some of these close pairs are separated by a nearly flat light section, as on 2013 April 30. Interestingly, 'accretion bursts' and possibly QPOs of much shorter period (11–30 min) and small amplitude ($\sim$0.01−0.05 mag) are often superimposed on primary ($\sim$0.1−0.5 mag) bursts in both rising and descending branches, or in the light maxima only. From time to time, we observe a significant accumulation of well-separated bursts occurring throughout the entire night: the variability may be either completely chaotic, as on 2013 April 22, or (nearly) periodic and possibly time-coherent, at least at first sight (e.g. 2014 March 9 and 2016 February 29). The lifetimes of such single oscillatory packages are merely 2–4 cycles. Amplitudes of these variations appear to scale as the whole light curve. They are highest in the ultraviolet, still clearly visible in the blue bands and usually only barely visible in the green and yellow parts of the spectrum. This is an important finding, as it limits the possible locations of their formation to hotspots and instabilities in the accretion process.

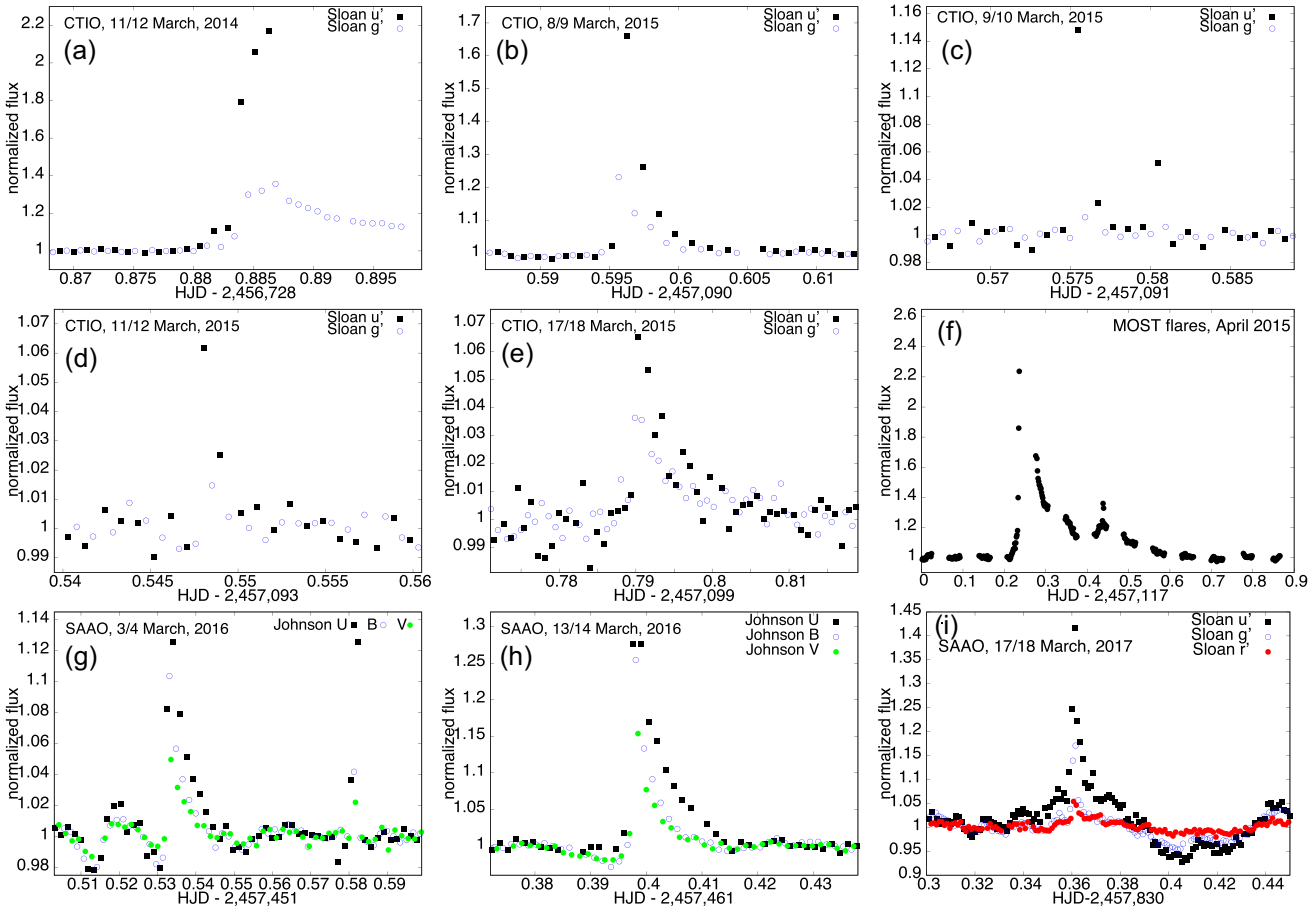

Figure 5. Enlargements of nine light-curve segments with 12 flares of TW Hya. Their intensities are expressed in underlying continuum flux units, which were estimated and removed by means of polynomial fits. The 2014 flare (first panel) appeared at twilight and was not observed completely. In three cases a secondary flare (or a flash) appeared soon after the primary one.

All of the above phenomena observed in TW Hya were already spotted and well characterized in BP Tau (a CTTS) by Gullbring et al. (1996). These authors explained these bursts as the result of inhomogeneous accretion, which is composed of numerous fragments that flow in a random way to the star (see section 7 in their article). Using realistic values of an accretion stream and the resulting hotspots, they calculated cooling times after the impacts of such fragments on the star, ranging from 30 min to several hours, which is in accord with their observations of the shortest bursts in BP Tau lasting for 0.6 h. They explained the range of rise times as dependent on the 'length' of the inhomogeneities in the accretion flow. Further 'shot-noise' simulations of light curves, binned appropriately for direct comparison with real observations, resulted in a range of peaks, either rounded (typical for variability observed almost 80 per cent of the time) or sharp-like (typical for 'accretion bursts' of 'triangular' shapes), or even others, having either linear rises followed by exponential decays or 'square' shapes, which are visible in the real photon-noised observations as an inverted '*U*'.

All the aforementioned structures can be easily identified in our light curves of TW Hya. This kind of variability, occurring on longer time-scales than investigated here, was already noticed by Rucinski et al. (2008). Here in Fig. 6 we present clear instances of such variations occurring on time-scales ranging from a dozen minutes to several hours.

3.5.2 *Fourier analysis*

To analyse the data from single nights with the Fourier technique, we removed nightly trends using second- to third-order polynomials. Thereafter magnitudes were transferred to fluxes, which were normalized to unity at the nightly mean star brightness levels, as shown in the left panels of Fig. 6 – the right panels show the corresponding periodograms obtained by a crude inversion of the amplitude–frequency spectra. Usually the blue bands (g', B filters) were analysed, as they provide the best ratio of variability amplitude to photometric accuracy of a single data point.

For illustrative purposes, in Fig. 6 we selected data obtained during eight representative nights. For example, during the first night (2013 April 11), long- and short-term superimposed oscillations coexisted at all times. The quasi-period of the longer variation was 1.6 h, while that of the shortest was apparently unstable, close to about 15 min. In addition, we observe a forest of peaks in the range 0.6–1 h. Similar coexisting short- and long-term variability was also observed during other nights.

The peaks visible in the periodograms do appear randomly in the Fourier spectra. We arrived at this conclusion using an average Fourier spectrum computed from all 16 individual Fourier spectra prepared from the u- and g'-band data, displayed on a logarithmic scale; the result for the u band is shown in Fig. 7. Instead, however, in actual fact they clearly show a flicker-noise dependence $a(f) \propto$

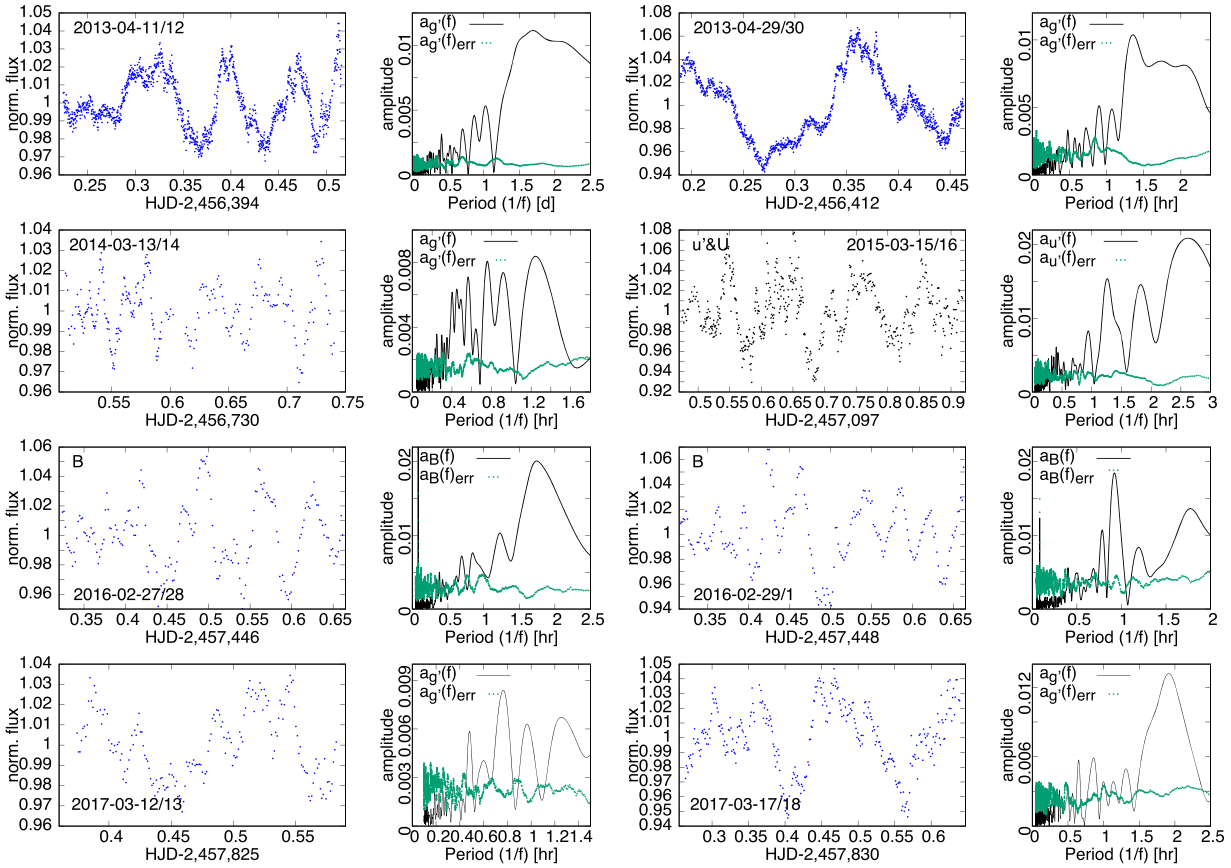

Figure 6. The g'-filter detrended light curves (left panels) obtained during nights when short-periodic QPOs were directly observed. They are expressed in flux units normalized to unity at the mean nightly levels. The periodograms are shown in the small right panels; the amplitudes of particular filter data, e.g. $a_{g'}(f)$, are expressed by continuous lines, while their errors are indicated by small dots. For the 2015 oscillations, combined u-band data and their oscillation spectra are also shown. B-filter light curves were used to investigate variability observed in 2016.

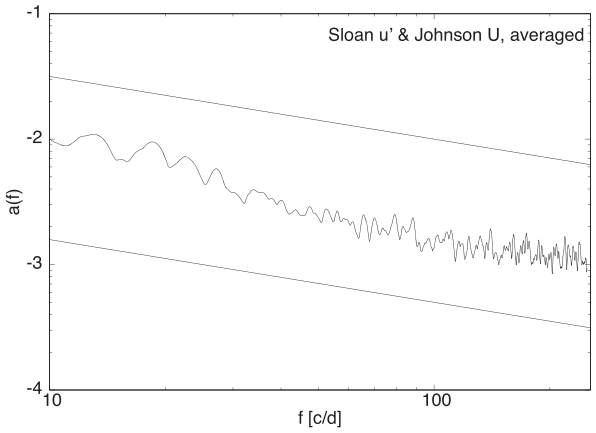

Figure 7. Averaged Fourier spectrum (computed from spectra obtained during 16 different nights) on a logarithmic scale. No distinct periodicities can be identified; instead the spectrum shows a pure flicker-noise character indicated by the two straight lines.

$\sqrt{f}$, indicated by the two straight lines. This result confirms the flicker-noise character of the short periodic variability in TW Hya for time-scales from minutes to hours, as was already proven for time-scales of days, weeks and years by Rucinski et al. (2008).

Except for the above cases, we also made dedicated searches for the shortest quasi-periodicities possible for detection with the 2013 g'-filter data, which were sampled every 10–23 seconds. However, they do not show any significant oscillations in the range 30 s–10 min.

3.5.3 *Wavelet analysis*

The lack of well-distinguished high-frequency peaks in the Fourier spectra appears to contrast with many clear instances of small-amplitude, possibly quasi-periodic variations in our light curves. Therefore we applied the wavelet technique for analysis of six representative nights. The original ground-based data were re-sampled with uniform steps (similar to the observing cadence during a given night) using the procedure previously applied to the *MOST* data (Section 3.2). As expected, the two-dimensional wavelet spectra shown in Fig. 8 are more informative than their one-dimensional counterparts: the spectra reveal a range of brief events, either limited to single or double brightening events or showing an oscillatory character extended over a significant fraction of a night. Period changes are noticeable in many cases, which may explain the lack of well-defined high-frequency peaks in the Fourier spectra.

The shortest significant peaks identified, both in the Fourier spectra and directly in the light curves, are at 0.008–0.02 d (11–30 min). The best defined oscillatory-like variations can easily be localized in the local maximum on 2015 March 15/16. They show a period change in the range 0.016–0.01 d (23–15 min). Similar short-term 11–15 min light variations are observed during many (but not all)

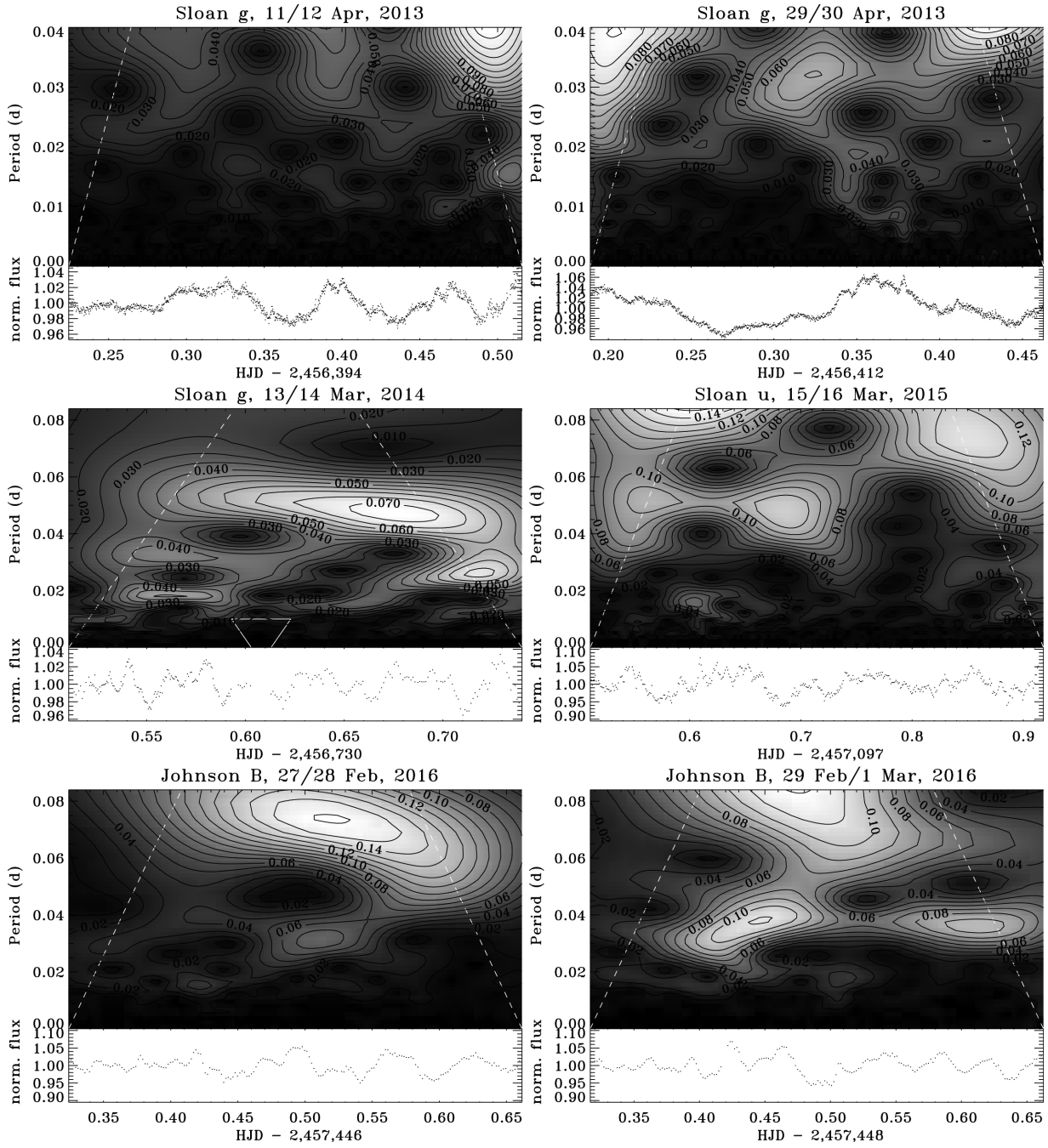

Figure 8. The wavelet spectra for a few selected nights. Events in the local maximum observed on 2015 March 15 show the best-defined signs of short-periodic oscillatory behaviour.

local maxima of 'accretion bursts'. Interestingly, we did not identify similar 11–15 min oscillations anywhere else in the light curves.

3.5.4 Discussion

The findings obtained from the wavelet analyses prompted us to consider an accretion shock instability as the possible cause of the formation of the shortest QPOs next to the 'accretion burst' scenario, which explains well light variations lasting longer than 0.5 hr.

According to Langer, Chanmugam & Shaviv (1981) and Chevalier & Imamura (1998), the fundamental mode of the thermal instability oscillation of an accretion shock has a characteristic period of the order of the cooling time of the post-shock gas and is mostly a function of electron density and different cooling functions (see section 4.1 of Drake et al. 2009 for details). The oscillations were searched for in CTTSs (including TW Hya) in the spectral range from X-rays to the Johnson *U* band, but the results of Drake et al. (2009) and Günther et al. (2010) were negative. The authors argued that oscillations arising simultaneously in a few hotspots can dampen each other and lead to negative detections. The authors of the second article were the first to search for these oscillations in the ultraviolet and blue bands, which pushed us to carry out similar searches in our data.

The shortest directly visible oscillations in our light curves, wavelet spectra and some periodograms are of period 11–20 min. This is much longer than the typical periods of 0.02–0.2 s predicted for CTTSs by Koldoba et al. (2008). However, our values are of the same order as the periods of ∼400 s predicted by Sacco et al. (2008), ∼500 s by Orlando et al. (2013) and 80–610 s by Costa et al. (2017). Although Matsakos et al. (2013) presented a range of models, among them one with an oblique impacting surface leading to QPOs of 15 min – very similar to those observed in TW Hya – the authors further argued that several perturbation types, such as clumps in the accretion stream or chromospheric fluctuations, may disrupt or even suppress expected oscillations.

We conclude that it is not clear whether the shortest light variations observed in TW Hya can be assigned to post-shock plasma oscillations. Apparently new observational tests should be devised to check the advantage of this mechanism also over hypothetical, well-organized inhomogeneous accretion of small clumps. We speculate that for some reason the clumps could hit the star at quite regular intervals, which would lead in turn to light variations mimicking oscillatory variations.

3.6 Colour indexes versus brightness variations

Although our data suffer from a lack of photometric calibrations to the standard Johnson and Sloan systems, they contain rich information about colour index versus brightness evolution of TW Hya both during whole runs and single nights. We prepared three colour–magnitude diagrams utilizing most of the 2014, 2015, 2016 and 2017 multicolour observations, corrected for atmospheric extinction effects (Fig. 9). Relations for individual nights are not important on these plots, but rather the general shape all these nights take when combined together.

In general, TW Hya becomes bluer when brighter, as is typical for CTTSs where accretion is the rule. One can note considerable spread of colour indices for a given magnitude on each diagram. This amounts to 0.3 mag in the $\Delta g' - \Delta(u' - g')$ relation, is slightly smaller (0.2 mag) in the $\Delta V - \Delta(U - V)$ diagram and becomes a factor of two smaller (0.1 mag) in the last $\Delta V - \Delta(B - V)$ relation. These spreads are far too large to be explained by any instrumental errors or imperfections in the atmospheric colour-extinction removal. Instead, they must be associated with the star or – more specifically – with the variety of hotspot parameters.

The effects discussed above were observed in TW Hya for the first time by Rucinski & Krautter (1983). Many other Type II T Tauri stars showed scatter in their colour indices based on *U*- and *B*-filter data by Herbst et al. (1994). Fernández & Eiroa (1996) explained this by the appearance of hotspots of different temperature. These authors found more concise colour–magnitude relations in diagrams based on *VR* filters, as they are less sensitive to variations in hotspot temperatures.

In order to illustrate this effect in TW Hya, we present a theoretical colour–magnitude diagram. We utilized the results of Calvet & Gullbring (1998), who calculated the structure of the accretion column in CTTSs and obtained surface filling factors by all shocks to be smaller than 10, typically 0.1–1 per cent. As the authors obtained typical hotspot temperatures of 6000–8000 K, we chose a mid-value of 7000 K during our computations. For comparison we also performed a second set of calculations assuming 10 000 K. We calculated synthetic magnitudes in *UBV* Johnson filters using the *PHOENIX* library of spectral intensities (Husser et al. 2013) and filter transmission curves from Bessel (1990). The effective temperature of the photosphere was assumed to be 4000 K and the respective intensity calculated for $\log g = 4.0$ was used during the stellar light integration. Appropriate linear limb-darkening coefficients in Johnson filters for a stellar photosphere and the considered hotspot temperatures were taken from Diaz-Cordoves, Claret & Gimenez (1995) and Claret, Diaz-Cordoves & Gimenez (1995).

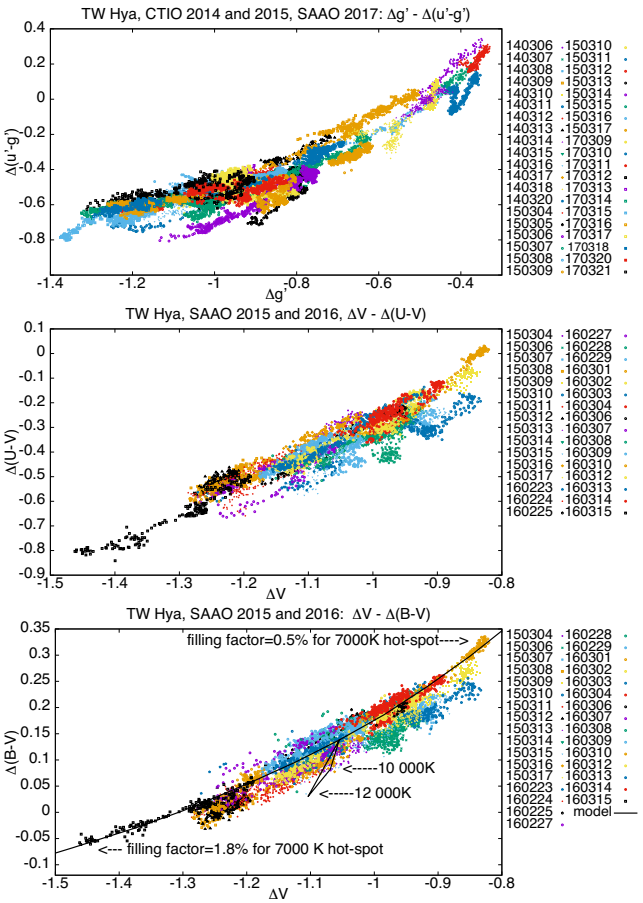

Figure 9. Colour–magnitude diagrams in Sloan and Johnson filters, composed of observations obtained during nights indicated in the legends (*yymmdd*). The differential magnitudes are computed with respect to the mean comparison star, computed from the first and third stars listed in Table 2. The theoretical diagram (namely 'model' in the legend) was manually matched only with the last diagram.

We started to compute a grid of synthetic magnitudes from an unspotted star. In the next step we added a small $1 \times 1\,\mathrm{deg}^2$ square hotspot on the observer's side of the star. Its size was increased by 1 deg in latitude and longitude in each consecutive step. As a result, we obtained the synthetic *UBV* magnitudes necessary for producing theoretical colour–magnitude diagrams. As our *SAAO* observations lack absolute calibrations, the theoretical diagram was adjusted manually to match the observed colour–magnitude relations closely. We found that the 'theoretical' hotspot responsible for the theoretical diagram that best matches our observations evolved in size either from 10×10 to $19 \times 19\,\mathrm{deg}^2$ for an effective temperature of 7000 K (as shown in the last panel in Fig. 9), or between 5×5 and $10 \times 10\,\mathrm{deg}^2$ assuming 10 000 K. Corresponding hotspot surface filling factors would then change from 0.5 to 1.8 or from 0.1 to 0.5 per cent, which is in accord with typical values of 0.1–1 per cent (Calvet & Gullbring 1998).

In the last step, we simulated the effect caused by the appearance of an additional hotspot of temperature higher than a typical value

of 7000 K. We considered single 2.5 × 2.5 deg^2 hotspots of two temperatures: first of 10 000 K and second of 12 000 K. The effects triggered by both hotspots are indicated on the last diagram by arrows. Once the additional hotspot light was 'switched off', the colour–magnitude relation changed to the original banana-shaped relation. This result is in accord with Fernández & Eiroa (1996) and may qualitatively explain the 'spread' observed in our diagrams.

The effect discussed above can also be illustrated well by diagrams specifically constructed for three particular nights, as shown in Fig. 10. They show effects triggered by the appearance of hotspots of apparently larger effective temperatures than that of an underlying hot continuum, leading to atypical behaviour in the colour–magnitude diagrams. To indicate the regions in the diagrams being disturbed by such hotspots, we decided to split the data obtained before, during and after the appearance of the hotspots and mark them with different colours and symbols.

(i) The first two left-hand panels in Fig. 10 shows data obtained at CTIO during 2014 March 11. The night can be also localized quickly in the first panel of Fig. 9, as the star was then in a low state of its brightness. Yet in the middle of the night its u'-filter brightness rose by 0.15 mag, while only 0.02–0.03 mag rise was noted in the g' filter at the same time.

(ii) The second example (the two middle panels) is from 2015 March 15, when the short (possibly) QPO considered as presumably due to post-shock plasma oscillations (Section 3.5) were noticed by us so clearly for the first time. Apparently, the hotspot associated with this QPO was of higher temperature than the mean temperature of the underlying hot continuum, since it added an extra 0.08 mag of ultraviolet light into the underlying relation.

(iii) The third example (the two right-hand panels) shows effects caused by two temporal hotspots ('accretion bursts') of 0.5–0.8 h duration observed during 2016 March 9. Interestingly, the $\Delta V - \Delta(B - V)$ relation remained stable, but the next one ($\Delta V - \Delta(U - V)$), which was more sensitive to the manifestation of additional hotspots with higher effective temperatures, showed two separate relationships.

We conclude that inhomogeneous accretion does not necessarily create hotspots with equal temperatures, as concluded by Gullbring et al. (1996). Apparently inhomogeneous accretion may also create hotspots hotter by 1000–5000 K from the assumed 'base level'. Our result is in qualitative accordance with Ingleby et al. (2013), who analysed ultraviolet and optical spectra of low-mass T Tauri stars assuming multiple accretion components. Only columns carrying 'high-energy fluxes' (3×10^{11} and 10^{12} erg s^{-1} cm^{-3}) with equal filling factors of 0.0013 (0.13 per cent) were found for TW Hya, as shown in table 5 of their article. According to the authors, these 'high-energy flux' columns may produce hotspots of effective temperatures up to 9000 K.

3.7 The search for occultations

The major motivation to conduct such an enormous observational effort from the ground was to investigate the mysterious occultations discovered in the 2011 *MOST* data of TW Hya. We were aware that this might be a risky venture, as previous space observations did not reveal any obvious similar events. Our first and minimal goal was to encounter occultations and check their spectral properties in at least two bands. In the best case, we expected to be able to determine their periodicity if they were sufficiently frequent in a particular season.

In Siwak et al. (2014), we temporarily concluded that these events could be due to hotspot occultations by hypothetical 'dusty clumps'. Assuming this scenario to be true, it would be advisable to estimate the physical conditions that would lead to the 2–3 per cent brightness drops observed by *MOST* in 2011 and calculate their depths in consecutive bands in e.g. the Johnson system. According to Kulkarni & Romanova (2008), the total number of unstable tongues at any given time is of the order of a few. Let us assume that the tongues created five hotspots with surface filling factors of about 0.7 or 0.1 per cent for the two already considered hotspot temperatures of 7000 and 10 000 K, respectively. Assuming that one of the spots is completely obscured by a hypothetical optically thick dusty clump, the light synthesis model (same as in Section 3.6) predicts a brightness decrease by 0.03–0.04 mag in the wide-band *MOST* and Johnson R_c filters, 0.07–0.09 mag in the V filter, 0.14–0.20 mag in the B filter and 0.2–0.27 mag in the U filter for both temperatures. Note that, in all bands but R_c, the expected depths are significantly higher than in the *MOST* band. Due to the fact that all the hypothetical hotspots were placed centrally on the observer's side of the star during the computations, slightly smaller light drops should be observed in practice, closer to 3 per cent for the *MOST* filter and in accord with the 2011 data. We note that the results of these calculations are sensitive functions of assumed hotspot temperatures, filling factors and occulted fraction and are slightly affected by the lack of emission lines (Dodin 2018) in the *PHOENIX* library of intensities, used in our simple model.

The best way to verify the above predictions would be to catch at least a single occultation with both *MOST* and the ground-based telescope. In spite of two simultaneous runs (2014, 2017),we were unfortunate that not even a single occultation was seen in the *MOST* data.

As described in Section 3.5, the ground-based data are dominated by 'accretion bursts' of various shapes and by possible QPOs occurring on time-scales from 11 min to several hours. They are superimposed on each other and resemble the artificial light curves simulated by Gullbring et al. (1996). Therefore one would come to the conclusion that, after sufficiently long monitoring, it should be possible to identify a fake occultation-like event due to the superposition of a few accretion-induced light effects.

Prejudiced about this possibility, we carefully studied all ground-based data. We checked light curves obtained differentially with respect to one or more comparison stars. We also examined the magnitudes of the variable and comparison stars separately to make sure that weather conditions were stable and/or the telescope mirror was not obscured by the edge of the dome, which usually leads to creation of fake light changes. We identified eight events (at least), which – according to the definition given in section 4.1 of Siwak et al. (2014) – could be classified as 'occultations'. We mark them in consecutive panels in Fig. 11.

The new events are definitely not as securely defined among surrounding variations as in 2011. The new events also have different characteristics from those seen in 2011.

(i) In contrast to the amazingly similar 2–3 per cent depths observed in 2011 by *MOST*, the new events show quite different behaviour, as illustrated in Table 3. They also exhibit much longer duration times between the outer (D) and inner (d) contacts. Nonetheless, the relation *branch duration versus total duration time* has amazingly similar slope (0.202 ± 0.018) to that obtained from the 2011 *MOST* data (0.199 ± 0.014), as shown in Fig. 12.

We note that only one event, #6 (2014 March 20), was similar in duration, depth and shape to event #3 observed by *MOST* in 2011.

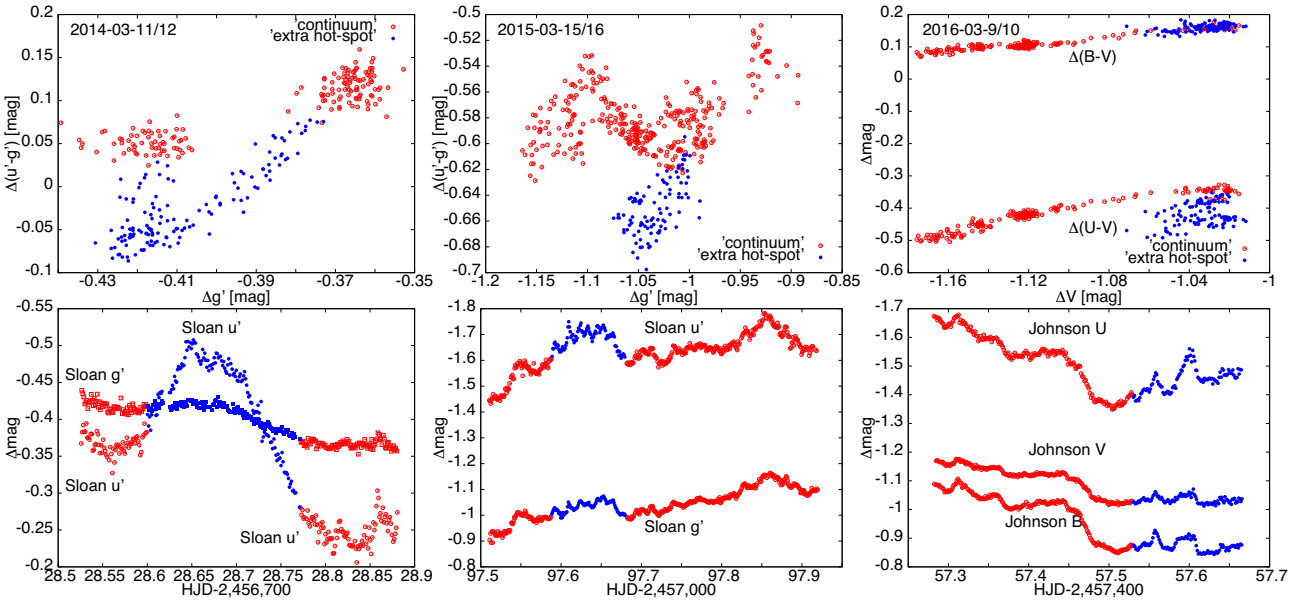

Figure 10. Colour–magnitude diagrams for three particular nights (upper panels) and respective fragments of light curves (bottom panels). Filled symbols represent data and corresponding colour indices obtained during additional hotspot appearances.

(ii) Most of the 2011 dips were observed in random places – only six events, marked in the 2011 light curve as #3, #13,#14, #15 (possibly), #17 and #18,occurred at or close to the local brightness maxima. In contrast, almost all new events appeared in the middle of the local brightness maxima. This is a very important finding, as it may indicate that they could be caused by total or partial hotspot light dimming, rather than by chance.

(iii) Assuming the above scenario to apply, we can estimate qualitatively whether a given occultation was total or partial. Whenever possible, we identified and approximately marked the positions (by 's' and 'e') at which hotspots associated with occultations appeared and disappeared among surrounding light variations. After that we drew a straight line between these positions. If the bottom of the occultation touched the line, we classified it as total. This is the case for events #2, #6and #8. Totality cannot be confirmed for events #3, #4, #5, #6and #7, as their bottoms fall much higher than the base light levels from which associated hotspots emerged. This indicates that the occulting bodies are not always fully optically thick.

(iv) Local brightness maxima observed in TW Hya are similar to the 'square' and 'triangular' features found in artificial light curves by Gullbring et al. (1996). Seven out of eight occultation-candidate events observed in TW Hya during 2013–2016 are localized in the middle of such light features. If these simulations included the possibility of hotspot occultation by fully or partially optically thick clumps ordered in an accretion stream, a brightness drop similar to that observed by us would be produced under favourable geometry. Note that in 2017 no event was noticed.

The dips observed in TW Hya are considerably shorter (15–90 min) and much shallower than those observed in AA Tau, which last for about a day. They are due to a warp arising near the disc corotation radius (Bouvier et al. 2003, 2007), in which optically thick disc plasma is lifted high enough above the disc plane to cause semi-periodic occultations of the star. Most recently, nine more similar semi-periodic dips were found in young stars in NGC 2264 by Stauffer et al. (2015). At least three of the stars are locked with the stellar rotation, which suggests the same mechanism as for AA Tau. Ten more similar stars were identified in *Kepler* spacecraft data for young members of the ρ Oph and Upper Sco star-forming regions by Ansdell et al. (2016). The unified models of these mechanisms were presented by McGinnis et al. (2015) and Bodman et al. (2017). The first group of authors estimated that the maximum warp height amounts to about 20–30 per cent of the disc radius at which it originates and may vary by 10–20 per cent on a time-scale of days, as inferred from analysis of consecutive occultations. The second group of authors added the possibility that the optical thickness of the warps decreases with their elevation over the disc mid-plane. These models do not foresee the possibility of occultations for CTTSs with low inclinations of visibility (as for TW Hya), but we speculate that remnant dust can perhaps be lifted high above the star to act as an occulting screen for hotspots revolving with an inner disc rotational frequency, as speculated in Siwak et al. (2014).

A similar hypothesis about tori of gas or dust levitating in remnant funnel flows (or trapped by the stellar magnetosphere) over high stellar latitudes was considered for a dozen weak-lined T Tauri stars (David et al. 2017; Stauffer et al. 2017) and for so called 'scallop-shell' stars (Stauffer et al. 2018). Though these stars do not reveal signs of accretion in their light curves, they show semi-periodic persistent flux dips lasting for a few hours, or just smooth flux variations confined to certain phases only. This hypothesis can also be considered for TW Hya, as absorption and scattering of *u*-band radiation by gas is much more efficient than at longer wavelengths, especially if emitted in the funnel stream direction. This scenario could explain especially well dips #4 and #5, which are significantlypronounced in the *u* band and separated by almost exactly 2 d and only barely visible in *the g′* filter, as well as the full or partial light dimming of the hotspots during remaining events.

'Occulting screens' described above could also be carried in equatorial tongues instead of a stable funnel, which is especially important for TW Hya, which does not necessarily always form a stable funnel flow. The plasma could first be transferred directly towards the star in a narrow tongue, which is ultimately wound along the stellar magnetic field lines and forms miniature funnel flows. The funnel flows impact the star at moderate latitudes (35–

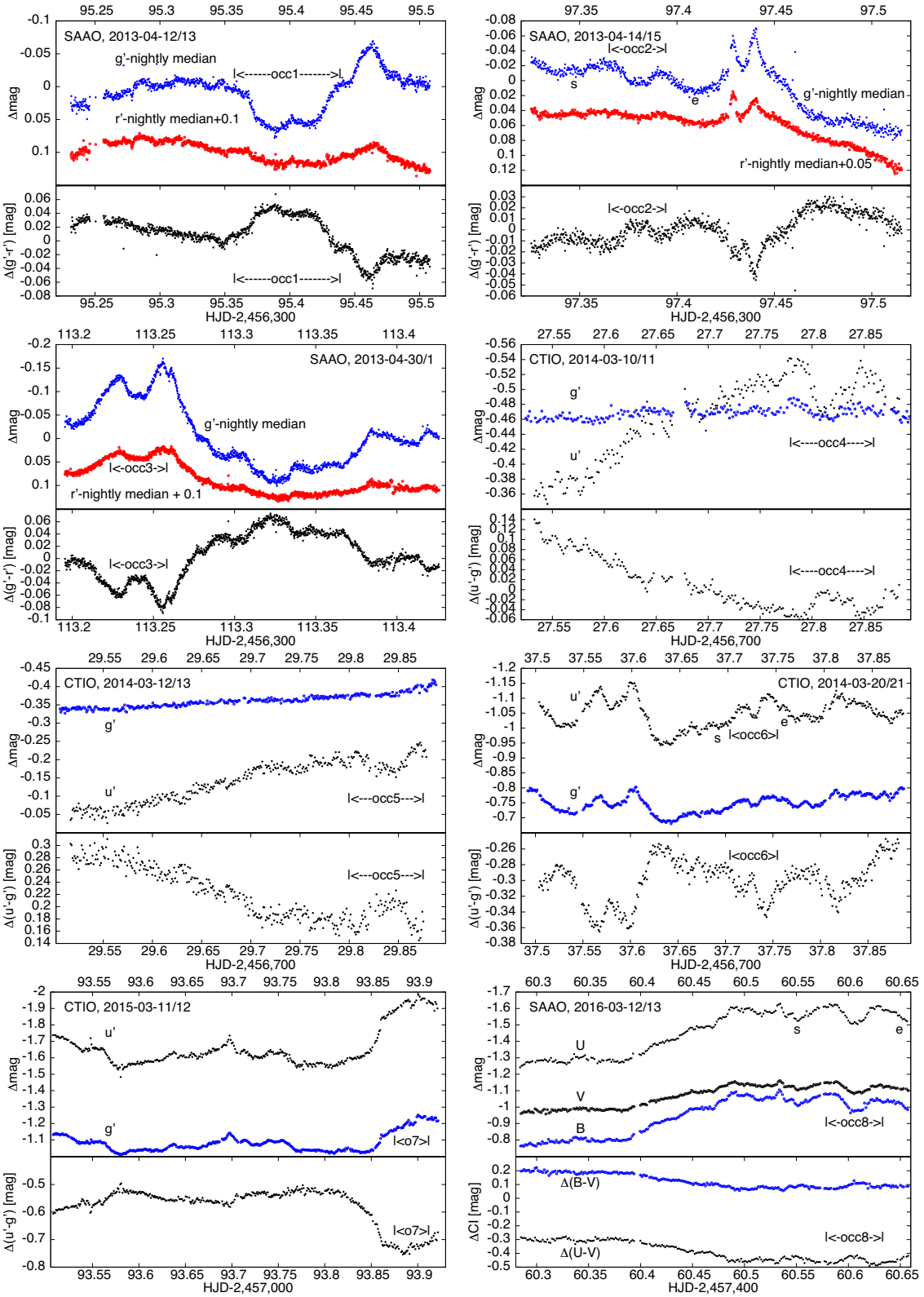

Figure 11. Possible occultations of hotspots in TW Hya, marked by ranges and numbers. The upper panels show light curves corrected for colour extinction, while the bottom panel shows colour index variations in time. Whenever possible, approximate moments when hotspots associated with the occultations appeared and disappeared in the light curves are marked by 's' and 'e', respectively.

Table 3. Basic properties of possible occultations: the central dip mid-times $hjd_{\rm min} = HJD-$ 245 6300 are estimated from the inner contacts with an uncertainty of 0.001 d. The depths are estimated in magnitudes, with an uncertainty of 0.004 mag, for appropriate filters. The outer D and inner d contact durations are in days; their typical uncertainty is 0.001 d (1.4 min).

No.	$hjd_{\rm min}$ [d]	Depth (band) [mag]	D [d]	d [d]
1	95.397	$g' = 0.056$ $r' = 0.014$	0.066	0.045
2	97.380	$g' = 0.024$ r' – undef	0.018	0.010
3	113.245	$g' = 0.062$ $r' = 0.022$	0.023	0.009
4	427.822	$u' = 0.074$ $g' = 0.014$	0.051	0.033
5	429.838	$u' = 0.059$ g' – undef	0.052	0.027
6	437.727	$u' = 0.059$ $g' = 0.024$	0.014	0.006
7	793.895	$u' = 0.044$ $g' = 0.044$	0.009	0.005
8	1160.609	$U = 0.106$ $B = 0.076$ $V = 0.067$	0.031	0.014

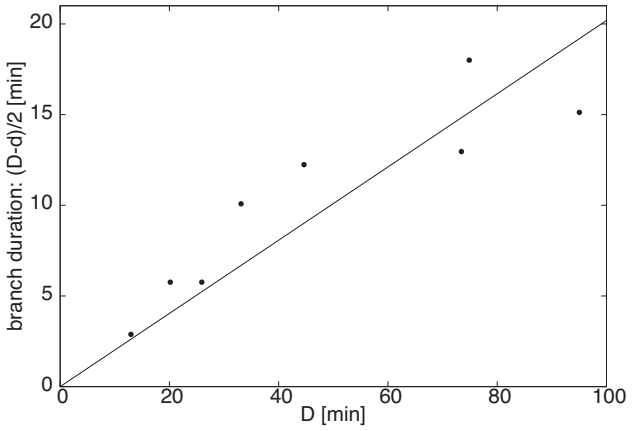

Figure 12. The relation (a straight-line fit) between the overall durations D and the branch durations $(D - d)/2$: $(D - d)/2 = 0.202(18)D$. The slope is very similar to that in 2011: 0.199(14).

65°: Romanova et al. 2008; Kulkarni & Romanova 2008, 2009) or even lower at 10–30°, as strictly constrained in TW Hya from X-ray observations by Argiroffi et al. (2017). The scenario with gaseous 'blobs' carried in the tongues may be considered as most promising (dust inside a magnetosphere should sublimate quickly) given the results obtained for other young stars and new indications for clumpy accretion in TW Hya, as discussed in Sections 3.5 and 3.6. This scenario would also explain the *occultation–local light maximum* connection naturally.

The last possibility is related to the fact that the 2011 events occurred during moderately stable accretion. According to Cranmer (2008), inhomogeneous clumpy accretion may add energy to waves in the photosphere. The waves show enhanced dissipation in polar regions through open polar flux tubes, which is sufficient to produce mass-loss rates of at least 0.01 times the accretion rate in the form of jet-like outflows. Whether or not the outflows could contain dusty clumps is also a matter of speculation.

4 SUMMARY

This is the last article utilizing new *MOST* data for TW Hya, due to the constantly decreasing efficiency of the satellite solar panels. The data were analysed together with ground-based high-quality multicolour observations, which enabled studies of subtle light changes on time-scales ranging from 30 s–5 yr. We considered a few topics, each described and immediately discussed in dedicated subsections of Section3. The major results can be summarized as follows.

(i) We confirm the primary finding from our last article (Siwak et al. 2014) that accretion in TW Hya switches between an unstable and a moderately stable state. In the moderately stable regime, quasi-periods caused by changing visibility of the major hotspot are observed. Although the new light curves were not as clearly dominated by equidistant peaks as in 2011, the values of 3.75 and 3.69 d observed in 2014 and 2017 are closer to the 3.57-d modulation induced in spectral lines by a persistent high-latitude cold-spot (Donati et al. 2011).

(ii) The new and important outcome from the ground-based observations is the characterization of the 'accretion burst' variability in TW Hya occurring on time-scales unavailable for *MOST*. Usually smooth light variations are observed, but they are often disturbed by single, two or even a series of strong 'accretion bursts'. The oscillation spectrum of these bursts has a flicker-noise character and no periodicity stable over many nights is indicated. Some of the variations may be time-coherent and quasi-periodic, as they appear at regular intervals not shorter than 11 min. The variations could be caused by inhomogeneous accretion, in which clumps ordered in the narrow accretion column hit the star in nearly regular intervals. Alternatively, the shortest 11–20 min light variations could be due to post-shock plasma oscillations.

(iii) We also analysed colour-index versus stellar-magnitude variations occurring within single nights and during several years. In particular, the comparison of colour–magnitude diagrams constructed from *UBV* data with theoretical diagrams resulting from a simple star and a hotspot light synthesis model indicates that these observations could be described by a hotspot of an average temperature of about 7000 K and filling factor varying between 0.5–1.8 per cent during the 2015 and 2016 SAAO runs. A similar relation with the assumed mean temperature of hotspots at 10 000 K results in a filling factor varying between 0.1 and 0.5 per cent. The complex colour–magnitude diagrams observed during a few particular nights can be assigned to short-term hotspots of effective temperatures that are 1000–5000 K higher than that of the basic hotspot continuum.

(iv) We also found 11 flares – a phenomenon common for many dwarf stars but only now observed in TW Hya. They are all of different amplitudes and duration times. The occurrence rate estimated for 2013–2017 indicates that the highest flaring activity is about one flare every two days during 2015–2016 but the significance of this result is low, as our monitoring lasted for barely 2–4 weeks each year. Still, this may give a first clue for the existence of a magnetic cycle similar to that of the Sun.

(v) The ground-based observations obtained in 2013–2017 at SAAO and CTIO were obtained with the intention to catch and characterize short and shallow light dips discovered in the 2011 light curve of this star (Siwak et al. 2014). Although at least eight occultation-like events can be indicated in our new data, we stress

that they are less securely defined among the surrounding light variations than in 2011 and may eventually turn out to be the result of an illusion caused by the superposition of 'accretion bursts'. However, new occultations are usually found in the local maxima of the stellar brightness. This finding prompted us to consider that these events may indeed be caused by occultations of hotspots by gaseous and/or dusty clumps transferred towards the star in the associated magnetized accretion tongues. High-cadence spectroscopic observations may help to verify this picture.

ACKNOWLEDGEMENTS

This study was based on data from the *MOST* satellite, a Canadian Space Agency mission jointly operated by Dynacon Inc., the University of Toronto Institute of Aerospace Studies and the University of British Columbia, with the assistance of the University of Vienna.

This article uses observations made at the South African Astronomical Observatory. MS and WO acknowledge Dr Hannah Worters and Dr Francois van Wyk for introduction to the SAAO telescopes and the entire observatory staff for the very generous time allocations and their hospitality.

This article uses observations made at the Cerro Tololo Inter-American Observatory at the 0.9-m telescope operated by the SMARTS Consortium. MS is grateful to Dr Jennifer G. Winters for help in efficient start of the CTIO run.

This article made use of NASA's Astrophysics Data System (ADS) Bibliographic Services.

This research has made use of the SIMBAD data base, operated at CDS, Strasbourg, France.

MS and WO are grateful to the Polish National Science Centre for grant 2012/05/E/ST9/03915. The Natural Sciences and Engineering Research Council of Canada supports the research of DBG, JMM, AFJM and SMR. Additional support for AFJM was provided by FQRNT (Québec). CC was supported by the Canadian Space Agency. TK, RK and WWW are supported by the Austrian Science Funding Agency (P22691-N16).

Polish participation in SALT is funded by grant No. MNiSW DIR/WK/2016/07.

Special thanks are also due to an anonymous referee for very useful suggestions and comments on the previous version of the article.

REFERENCES

Akiyama E. et al., 2015, ApJL, 802, 2
Alencar S. H. P., Batalha C., 2002, ApJ, 571, 378
Alencar S. H. P. et al., 2010, A&A, 519, 88
Andrews S. M. et al., 2016, ApJL, 820, 40
Ansdell M. et al., 2016, ApJ, 816, 69
Argiroffi C., Drake J. J., Bonito R., Orlando S., Peres G., Miceli M., 2017, A&A, 607, 14
Barrado y Nevescues D., 2006, A&A, 459, 511
Batalha C., Batalha N. M., Alencar S. H. P., Lopes D. F., Duarte E. S., 2002, ApJ, 580, 343
Bessel M. S., 1990, PASP, 102, 1181
Blinova A. A., Romanova M. M., Lovelace R. V. E., 2016, MNRAS, 459, 2354
Bodman E. H. L., Quillen A. C., Ansdell M., Hippke M., Boyajian T. S., 2017, MNRAS, 470, 202
Bouvier J. et al., 2007, A&A, 463, 1017
Bouvier J. et al., 2003, A&A, 409, 169
Calvet N., Gullbring E., 1998, ApJ, 509, 802
Chevalier R. A., Imamura J. N., 1982, ApJ, 261, 543
Claret A., Diaz-Cordoves J., Gimenez A., 1995, A&AS, 114, 247
Cody A. M. et al., 2014, AJ, 147, 82
Costa G., Orlando S., Peres G., Argiroffi C., Bonito R., 2017, A&A, 597, 1
Cranmer S. C., 2008, ApJ, 689, 316
David T. J. et al., 2017, ApJ, 835, 168
Debes J. H., Jang-Condell H., Weinberger A. J., Roberge A., Schneider G., 2013, ApJ, 771, 45
Debes J. H. et al., 2017, ApJ, 835, 205
Diaz-Cordoves J., Claret A., Gimenez A., 1995, A&AS, 110, 329
Dodin A., 2018, MNRAS, 475, 4367
Donati J.-F. et al., 2011, MNRAS, 417, 472
Drake J. J., Ratzlaff P. W., Martin Laming J., Raymond J., 2009, ApJ, 703, 1224
Fernández M., Eiroa C., 1996, A&A, 310, 143
Fukugita M., Ichikawa T., Gunn J. E., Doi M., Shimasaku K., Schneider D. P., 1996, AJ, 111, 1748
Gaia Collaboration et al., 2016, A&A, 595, A1
Grankin K. N., Melnikov S. Yu., Bouvier J., Herbst W., Shevchenko V. S., 2007, A&A, 461, 183
Gullbring E., Barwig H., Chen P. S., Gahm G. F., Bao M. X., 1996, A&A, 307, 791
Günther H. M. et al., 2010, A&A, 518, A54
Herbst W., Herbst D. K., Grossman E. J., Weinstein D., 1994, AJ, 108, 1906
Herbst W., Koret D. L., 1988, AJ, 96, 1949
Herczeg G. J., Wood B. E., Linsky J. L., Valenti J. A., Johns-Krull C. M., 2004, ApJ, 607, 369
Husser T.-O., Wende-von Berg S., Dreizler S., Homeier D., Reiners A., Barman T., Hauschildt P. H., 2013, A&A, 553, A6
Ingleby L. et al., 2013, ApJ, 767, 112
Kastner J. H., Zuckerman B., Weintraub D. A., Forveille T., 1997, Science, 277, 67
Koldoba A. V., Ustyugova G. V., Romanova M. M., Lovelace R. V. E., 2008, MNRAS, 388, 357
Kulkarni A. K., Romanova M. M., 2008, MNRAS, 386, 673
Kulkarni A. K., Romanova M. M., 2009, MNRAS, 398, 701
Kurosawa R., Romanova M. M., 2013, MNRAS, 431, 2673
Königl A., 1991, ApJ, 370, L39
Langer S. H., Chanmugam G., Shaviv G., 1981, ApJ, 245, L23
Lawson W. A., Crause L. A., 2005, MNRAS, 357, 1399
Matsakos T. et al., 2013, A&A, 557, A69
Matthews J. M., Kusching R., Guenther D. B., Walker G. A. H., Moffat A. F. J., Rucinski S. M., Sasselov D., Weiss W. W., 2004, Nature, 430, 51
McGinnis P. T. et al., 2015, A&A, 577, A11
Mekkaden M. V., 1998, A&A, 340, 135
Motl D., 2011, http://c-munipack.sourceforge.net
Munari U. et al., 2014, AJ, 148, 81
Orlando S. et al., 2013, A&A, 559, A127
Robinson C. E., Owen J. E., Espaillat C. C., Adams F. C., 2017, ApJ, 238, 100
Romanova M. M., Kulkarni A. K., 2009, MNRAS, 398, 1105
Romanova M. M., Kulkarni A. K., Lovelace R. V. E., 2008, ApJ, 673, L171
Romanova M. M., Ustyugova G. V., Koldoba A. V., Lovelace R. V. E., 2004, ApJ, 610, 920
Ruane G. et al., 2017, AJ, 154, 73
Rucinski S. M., 1988, Inf. Bull. Variable Stars, 3146, 1
Rucinski S. M., Krautter J., 1983, A&A, 121, 217
Rucinski S. M. et al., 2008, MNRAS, 391, 1913
Sacco G. G., Argiroffi C., Orlando S., Maggio A., Peres G., Reale F., 2008, A&A, 491, L17
Siwak M. et al., 2011, MNRAS, 410, 2725
Siwak M. et al., 2014, MNRAS, 444, 327
Siwak M. et al., 2016, MNRAS, 456, 3972
Stauffer J. et al., 2014, AJ, 147, 83
Stauffer J. et al., 2015, AJ, 149, 130
Stauffer J. et al., 2017, AJ, 153, 152
Stauffer J. et al., 2018, AJ, 155, 63
Stetson P. B., 1987, PASP, 99, 191

Tofflemire B. M., Mathieu R. D., Herczeg G. J., Akeson R. L., Ciardi D. R., 2017, ApJ, 842, 12
Uyama T., Tanigawa T., Hashimoto J., Tamura M., Aoyama Y., Brandt T. D., Ishizuka M., 2017, AJ, 154, 90
Walker G. A. H. et al., 2003, PASP, 115, 1023
Warmels R. H., 1991, PASP Conf. Series, 25, 115

APPENDIX A: EXTINCTION CORRECTIONS OF LIGHT CURVES

Due to the close proximity of TW Hya and both comparison stars (4 arcmin), differential extinction effects are negligible and were unaccounted for. However, in spite of very similar colour indexes of comparison stars and TW Hya, the variations of airmass X and colour indices of TW Hya itself do affect our nightly results ($\Delta U_{\rm obs}$, $\Delta B_{\rm obs}$, $\Delta V_{\rm obs}$, $\Delta u'_{\rm obs}$, $\Delta g'_{\rm obs}$) to a measurable extent – correction of the colour extinction term can eliminate most of these harmful effects.

We used the mean colour extinction coefficients β evaluated for SAAO and CTIO from Fukugita et al. (1996) and Mt Palomar sites; the values used in this work are as follows: −0.06, −0.052, −0.031, −0.02, −0.01, −0.008 for U, u', B, g', V, r' filters, respectively. TW Hya changes its colour indices significantly within each night. To follow these changes, we first interpolated V-filter differential magnitudes to obtain $\Delta V^{\rm int}_{\rm obs}$ at the moment of observations in the B filter (and vice versa). Then we obtained the corrected differential magnitudes using the colour equation limited to the colour extinction term:

$$\Delta B_{\rm corr} = \Delta B_{\rm obs} - \beta_B \times (\Delta B_{\rm obs} - \Delta V^{\rm int}_{\rm obs}) \times X_B,$$

$$\Delta V_{\rm corr} = \Delta V_{\rm obs} - \beta_V \times (\Delta B^{\rm int}_{\rm obs} - \Delta V_{\rm obs}) \times X_V.$$

Finally, we corrected observations in the U filter:

$$\Delta U_{\rm corr} = \Delta U_{\rm obs} - \beta_U \times (\Delta U_{\rm obs} - \Delta B^{\rm int}_{\rm corr}) \times X_U,$$

where $\Delta B^{\rm int}_{\rm corr}$ are the B-filter magnitudes corrected above, interpolated for the moment of the U-filter observations. These equations automatically account for differences between the colour indices of TW Hya and comparison stars. X_U, X_B, X_V denote airmasses for the indicated filters, calculated for the moments of mid-exposure. An analogous procedure was applied to correct the data obtained in the Sloan filters:

$$\Delta u'_{\rm corr} = \Delta u'_{\rm obs} - \beta_{u'} \times (\Delta u'_{\rm obs} - \Delta g'^{\rm int}_{\rm obs}) \times X_{u'},$$

$$\Delta g'_{\rm corr} = \Delta g'_{\rm obs} - \beta_{g'} \times (\Delta u'^{\rm int}_{\rm obs} - \Delta g'_{\rm obs}) \times X_{g'}.$$

These results were used to construct reliable (though still left in the instrumental systems) colour–magnitude diagrams, i.e. $\Delta(B_{\rm corr} - V_{\rm corr})$, $\Delta(U_{\rm corr} - V_{\rm corr})$ and $\Delta(u'_{\rm corr} - g'_{\rm corr})$, as shown in Figs 9 and 10, and for investigation of long-term variability of TW Hya in Section 3.3 (Fig. 2h,i).

The instrumental raw data points for TW Hya ($m_{\rm obs}$) obtained at the SAAO with TRIPOL (Section 2.2.1) during photometric nights in the $g'r'$ filters were corrected approximately on nightly trends by means of the following equation:

$$m_{\rm corr} = m_{\rm obs} - k \times X - \beta \times (g' - r') \times X,$$

where differential extinction coefficients k were assumed equal to +0.22 and +0.1 for the g' and r' filters, respectively, while β coefficients were the same as used above. The constant value of $(g' - r') \approx 1.22$ taken from the SIMBAD data base was used in this process. The results for the g' filter are shown in Fig. B1, but were earlier used in transformed light curves in Figs 6, 8 and 11.

APPENDIX B: THE SAAO AND CTIO LIGHT CURVES

We show here in details observations obtained during individual photometric-quality (and sometimes also partly cloudy) nights over 2013-2017. Only nights when the monitoring lasted longer than a few hours are shown. In Fig. B1 we show data obtained in g'-filter during photometric nights only. No comparison star was used to produce these light curves. Instead, the extinction-related nightly trends were removed, as described in Appendix A. In Figs B2-B6 we show light curves obtained at CTIO and SAAO during 2014-2017 runs. These light curves were obtained with respect to a 'mean comparison star' and are left uncorrected for atmospheric extinction effects for reasons described in Section 2.2.3.

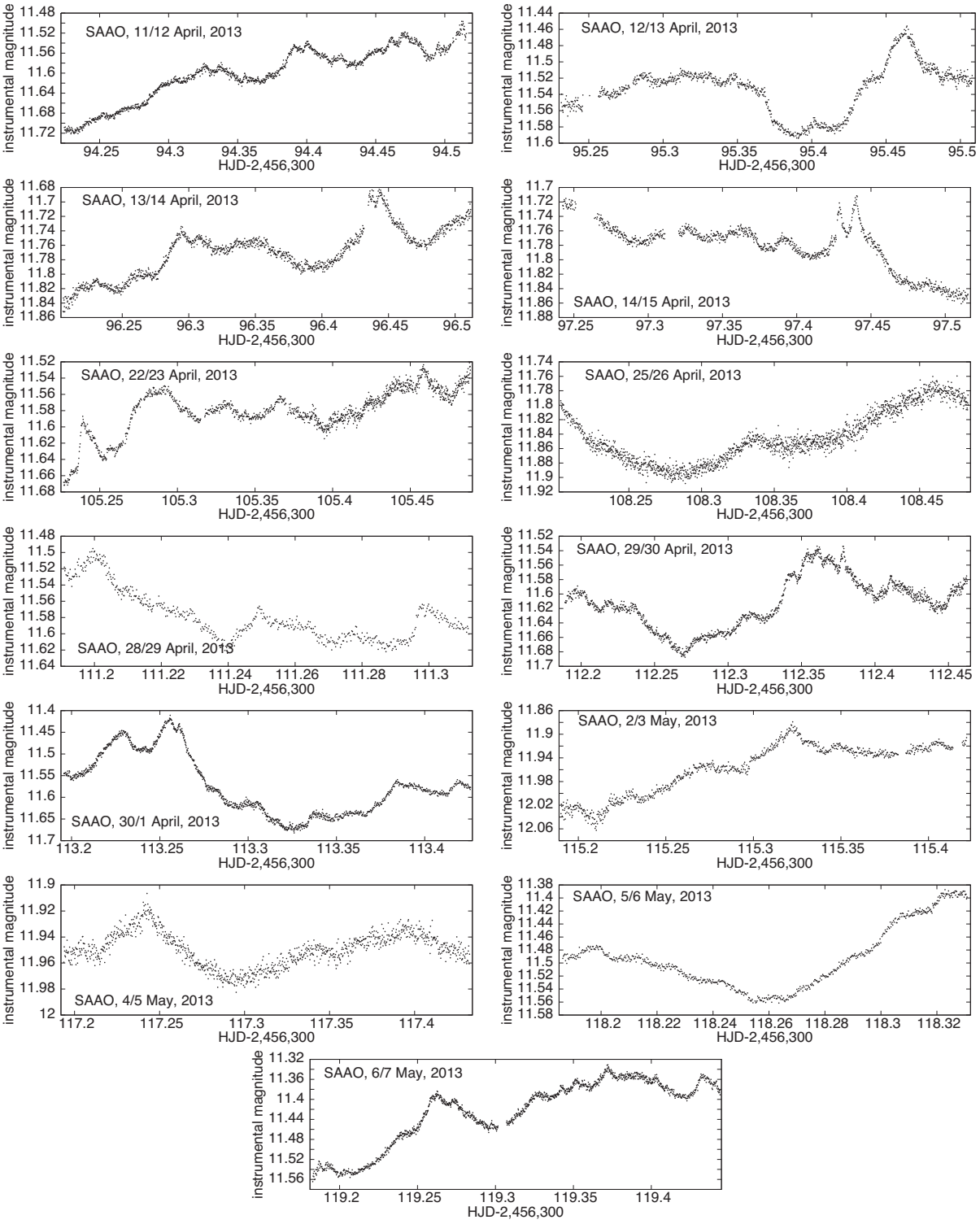

Figure B1. The g'-filter data obtained in 2013 at SAAO during photometric nights. The data are expressed at an arbitrary magnitude level due to the lack of a good comparison star. The nightly trends were removed using mean atmospheric extinction coefficients (see Appendix A).

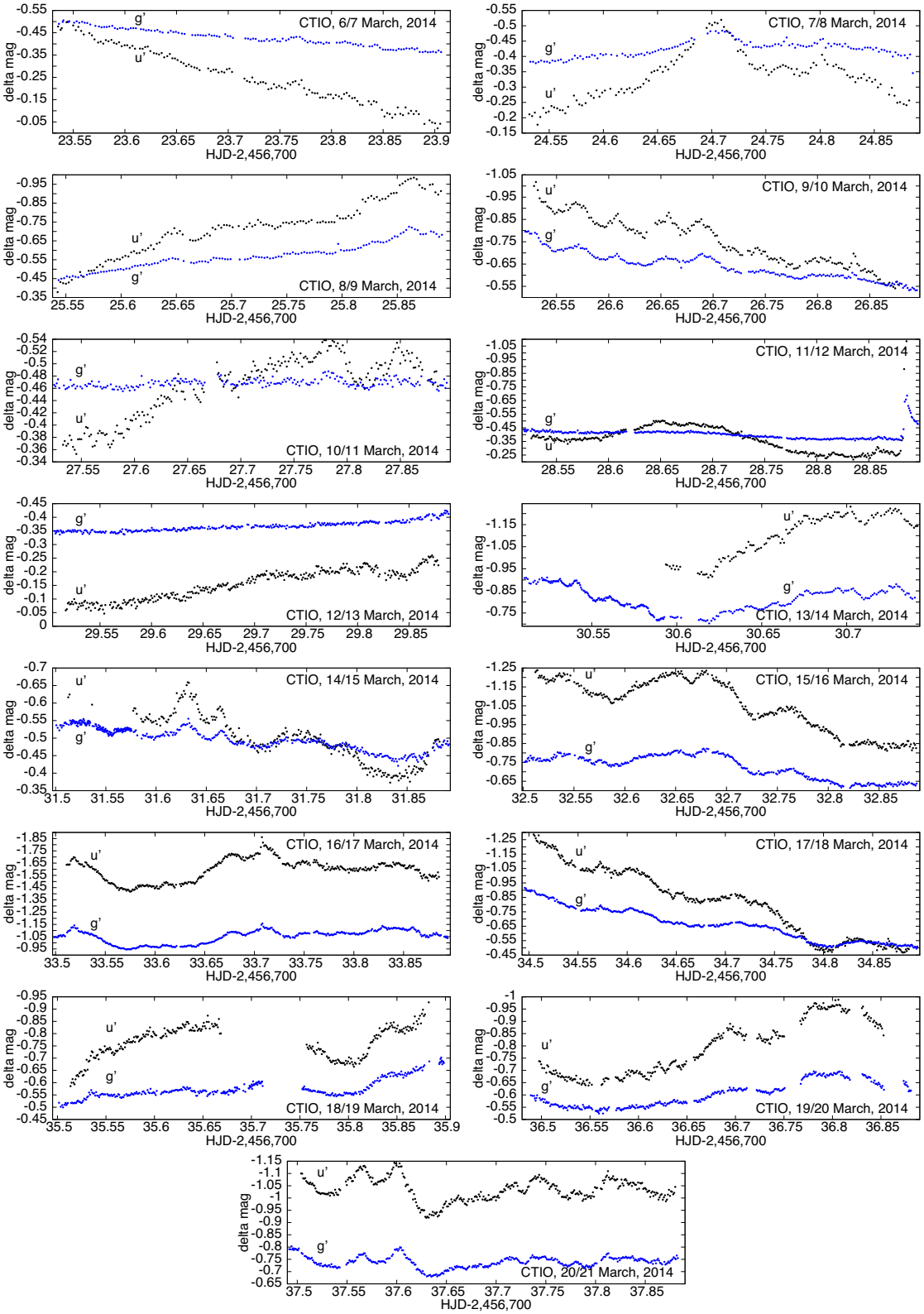

Figure B2. The u'- and g'-filterdata obtained at CTIO in 2014 with respect to the first and third comparison stars from Table 2. The data were left in the instrumental system uncorrected for atmospheric extinction effects.

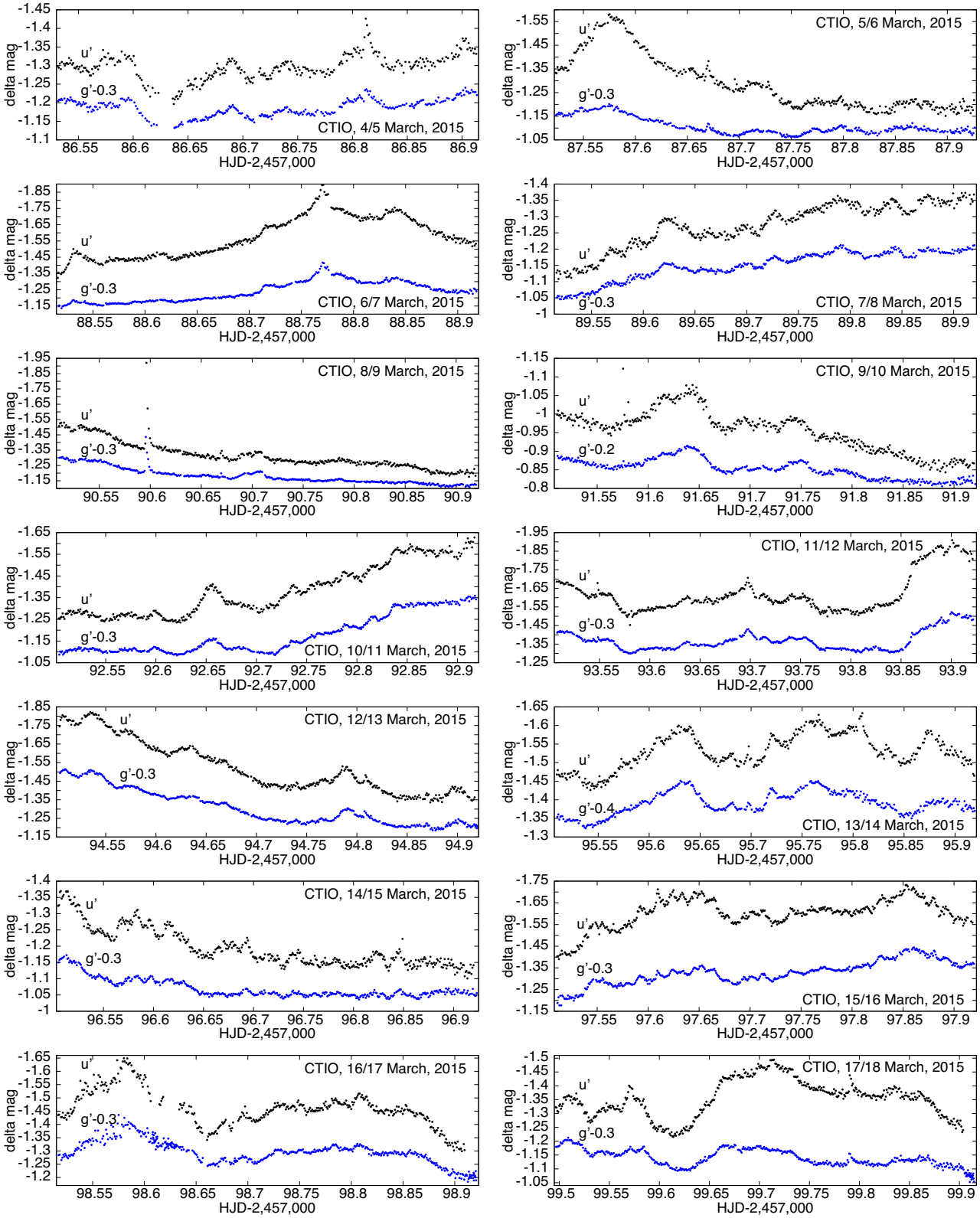

Figure B3. The u'- and g'-filterdata obtained at CTIO in 2015 with respect to the first and third comparison stars from Table 2. The data were left in the instrumental system uncorrected for atmospheric extinction effects. In contrast to the previous run, the g'-filter light curves were shifted by the indicated value for clarity.

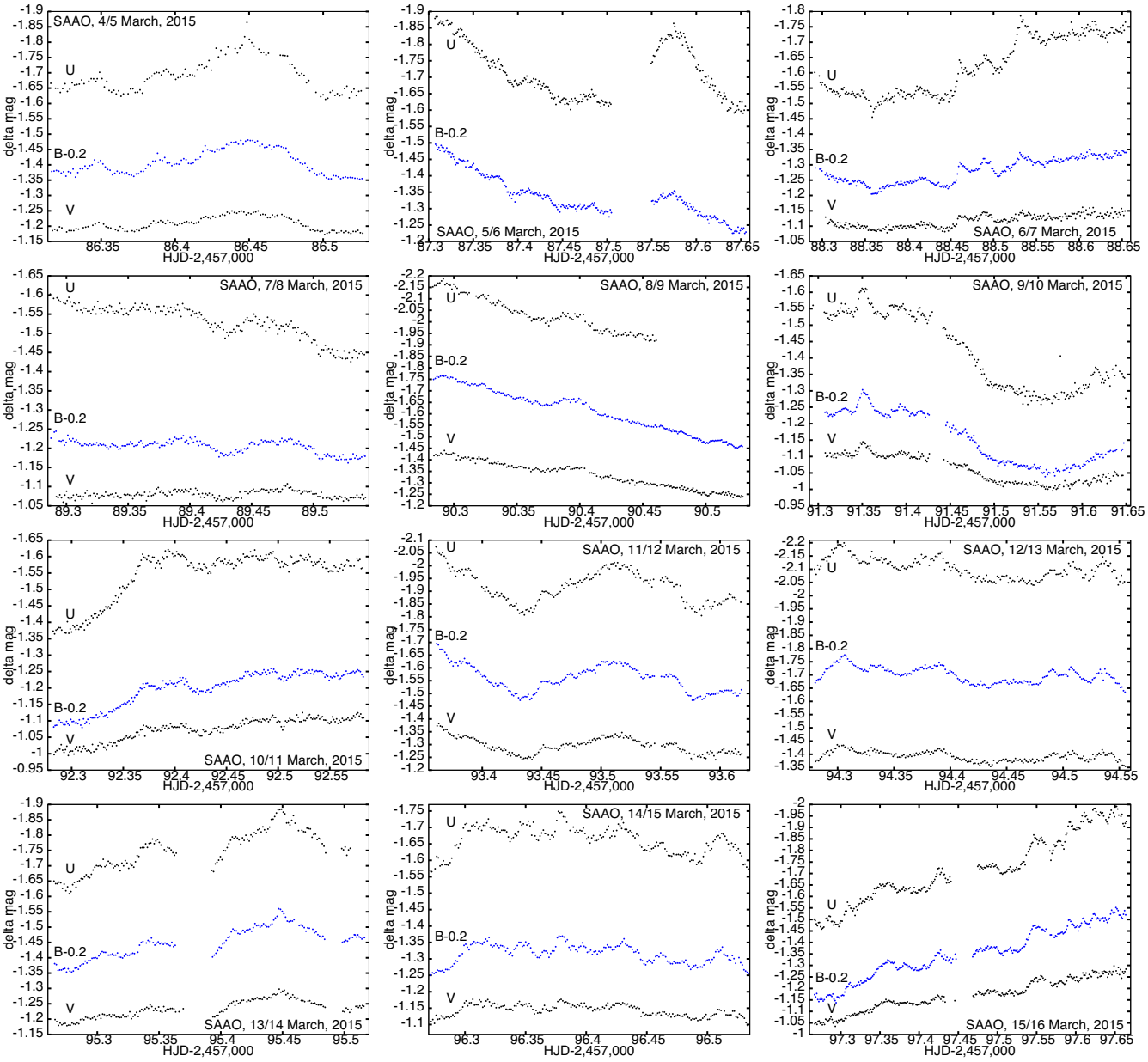

Figure B4. The *UBV* light curves obtained at SAAO in 2015. The light curves were obtained with respect to the first and second comparison stars from Table 2 and were left in the instrumental system uncorrected for atmospheric extinction. Only runs lasting longer than 3 h are shown.

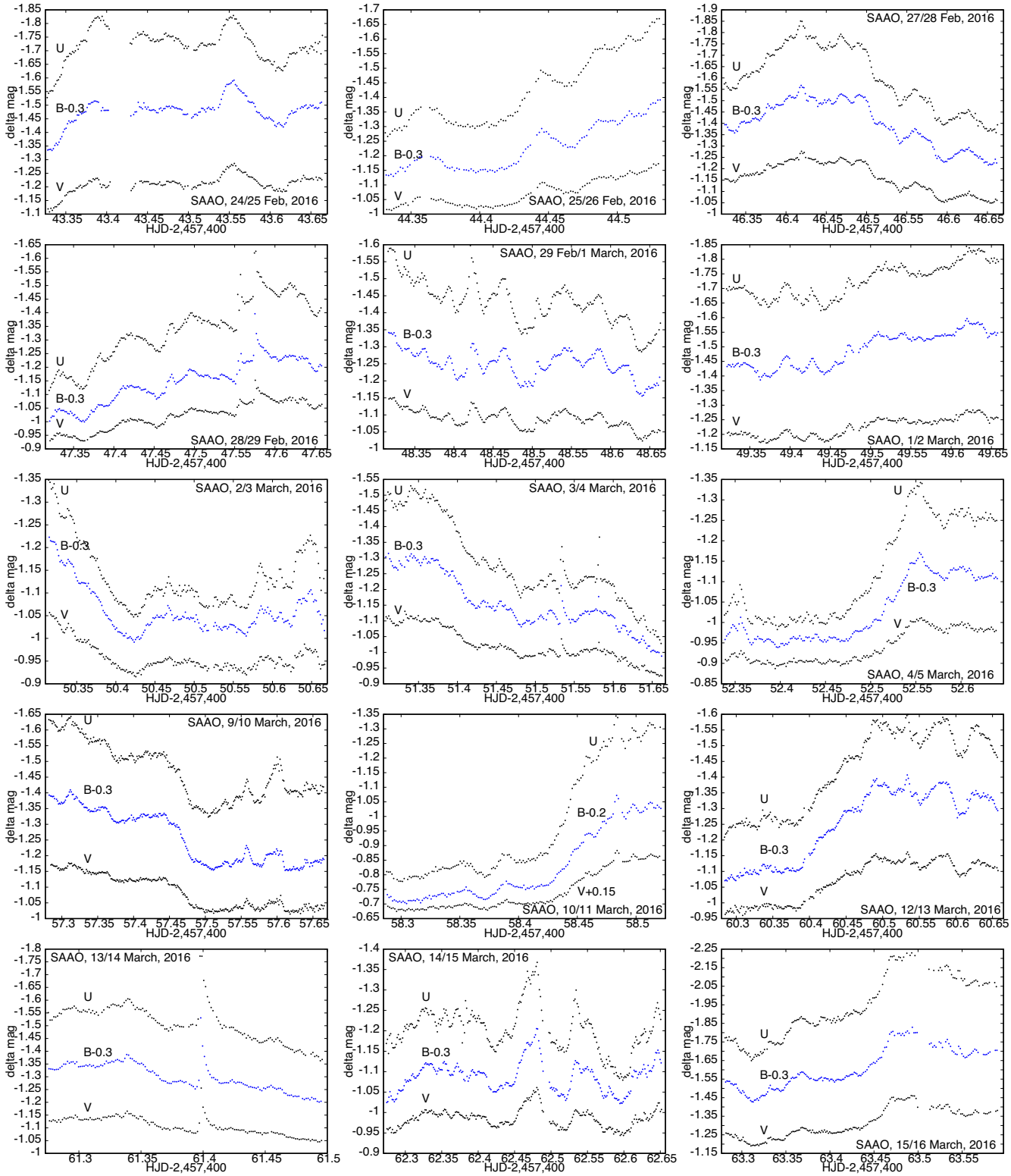

Figure B5. The *UBV* light curves obtained at SAAO in 2016. The light curves were obtained with respect to the first and third comparison stars from Table 2 and were left in the instrumental system uncorrected for atmospheric extinction. Only runs lasting longer than 3 h are shown.

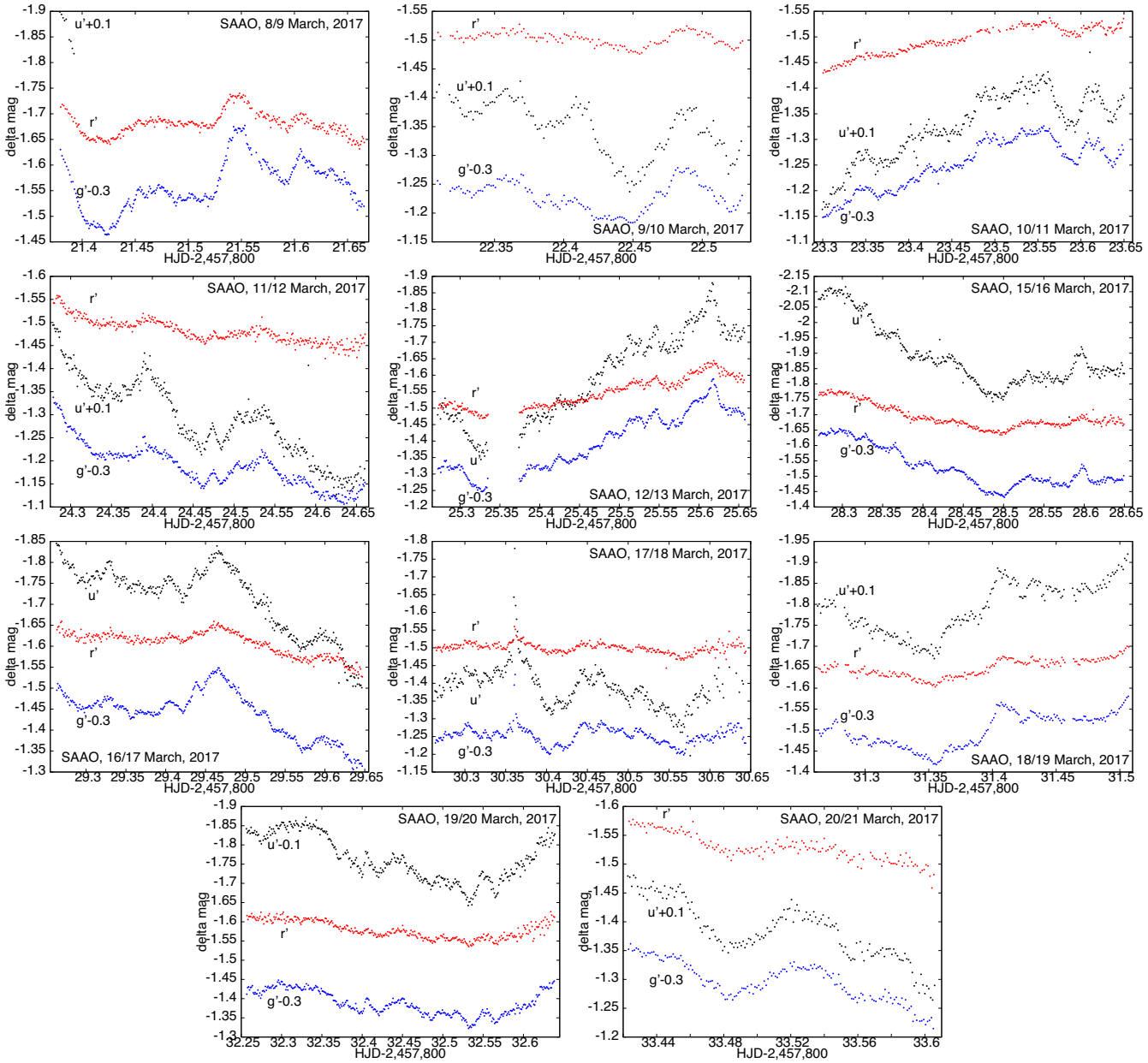

Figure B6. The $u'g'r'$ data obtained at SAAO in 2017 with respect to the first and third comparison stars from Table 2. Data obtained both during photometric and partly cloudy nights are shown. The data were left in the instrumental system uncorrected for atmospheric extinction effects. A shift in the magnitude scale is sometimes added for clarity.

This paper has been typeset from a TEX/LATEX file prepared by the author.